














The 2022–2023 accretion outburst of the young star V1741 Sgr

Michael A. Kuhn ¹★, Lynne A. Hillenbrand,² Michael S. Connelley ³, R. Michael Rich ⁴,
Bart Staels ⁵, Adolfo S. Carvalho ², Philip W. Lucas ¹, Christoffer Fremling ², Viraj
R. Karambelkar ², Ellen Lee,³ Tomás Ahumada ², Emille E. O. Ishida ⁶, Kishalay De ⁷,
Rafael S. de Souza ¹ and Mansi M. Kasliwal ²

¹Centre for Astrophysics Research, Department of Physics, Astronomy and Mathematics, University of Hertfordshire, Hatfield, AL10 9AB, UK

²Department of Astronomy, California Institute of Technology, 1216 East California Boulevard, Pasadena, CA 91125, USA

³University of Hawaii at Manoa, Institute for Astronomy, 640 North Aohoku Place, Hilo, HI 96720, USA

⁴Department of Physics & Astronomy, University of California Los Angeles, PAB 430 Portola Plaza, Los Angeles, CA 90095-1547, USA

⁵American Association of Variable Star Observers, 185 Alewife Brook Parkway, Suite 410, Cambridge, MA 02138, USA

⁶Université Clermont Auvergne, CNRS/IN2P3, LPC, F-63000 Clermont-Ferrand, France

⁷Kavli Institute for Astrophysics and Space Research, Massachusetts Institute of Technology, Cambridge, MA, USA

Accepted 2024 January 11. Received 2024 January 11; in original form 2023 July 10

ABSTRACT

V1741 Sgr (= SPICY 71482/Gaia22dtk) is a Classical T Tauri star on the outskirts of the Lagoon Nebula. After at least a decade of stability, in mid-2022, the optical source brightened by ~ 3 mag over 2 months, remained bright until early 2023, then dimmed erratically over the next 4 months. This event was monitored with optical and infrared spectroscopy and photometry. Spectra from the peak (October 2022) indicate an EX Lup-type (EXor) accretion outburst, with strong emission from H I, He I, and Ca II lines and CO bands. At this stage, spectroscopic absorption features indicated a temperature of $T \sim 4750$ K with low-gravity lines (e.g. Ba II and Sr II). By April 2023, with the outburst beginning to dim, strong TiO absorption appeared, indicating a cooler $T \sim 3600$ K temperature. However, once the source had returned to its pre-outburst flux in August 2023, the TiO absorption and the CO emission disappeared. When the star went into outburst, the source's spectral energy distribution became flatter, leading to bluer colours at wavelengths shorter than ~ 1.6 μm and redder colours at longer wavelengths. The brightening requires a continuum emitting area larger than the stellar surface, likely from optically thick circumstellar gas with cooler surface layers producing the absorption features. Additional contributions to the outburst spectrum may include blue excess from hotspots on the stellar surface, emission lines from diffuse gas, and reprocessed emission from the dust disc. Cooling of the circumstellar gas would explain the appearance of TiO, which subsequently disappeared once this gas had faded and the stellar spectrum reemerged.

Key words: accretion, accretion discs – techniques: spectroscopic – stars: individual: V1741 Sgr – stars: pre-main-sequence – stars: variables: T Tauri, Herbig Ae/Be.

1 INTRODUCTION

Accretion onto young stellar objects (YSO) leads to a wide range of variable behaviours, from low-amplitude variations on time-scales of days to weeks, to outbursts of several magnitudes lasting months to decades. Traditionally, outbursts have been divided into two phenomenological classes: the FU Ori class, whose outbursts last many decades and have a distinct absorption spectral signature, and the EX Lup class (also known as EXors), whose outbursts last months or years and exhibit atomic and molecular emission features (Hartmann & Kenyon 1996; Audard et al. 2014). Nevertheless, there is considerable diversity in the light curves and spectra of these accretion outbursts, suggesting the possibility of additional classes and/or a behavioural continuum (Fischer et al. 2023; Semkov 2023). EX Lup-type stars, in particular, display considerable variation in the strengths of their emission features (e.g. Giannini et al. 2022).

Furthermore, some YSO outbursts display mixed FU Ori and EX Lup-like features (e.g. Contreras Peña et al. 2017b; Connelley & Reipurth 2018; Hillenbrand et al. 2022a), whereas others have nearly featureless spectra (e.g. Lucas et al. 2020; Wang et al. 2023).

The collection of well-characterized outbursts is still relatively small and only sparsely samples the range of possible outburst behaviours and spectral properties. This poses challenges to refining classifications and, thereby, our physical understanding of these events. Recent discovery rates range from one to several per year, mainly from time-domain surveys monitoring large areas of the sky (e.g. Hillenbrand et al. 2021; Cruz-Sáenz de Miera et al. 2022; Park et al. 2022; Contreras Peña et al. 2023a, b). However, historical discovery rates have been much lower. Furthermore, the characterization of EX Lup-type outbursts at their peak requires relatively quick follow-up spectroscopy, meaning that rapid identification of outbursts is essential.

Here, we discuss a year-long EX Lup-type outburst from the Classical T Tauri star V1741 Sgr ($18^{\text{h}} 02^{\text{m}} 14^{\text{s}}.3 - 24^{\circ} 03' 47''$). This

* E-mail: m.kuhn@herts.ac.uk

source was first noted as a variable star in the vicinity of the Lagoon Nebula by Walker (1957).¹ However, observers paid it little attention in the subsequent decades. More recently, its infrared excess was detected in Spitzer/Infrared Array Camera (IRAC; Fazio et al. 2004; Werner et al. 2004) photometry from the Galactic Legacy Infrared Midplane Survey Extraordinaire (GLIMPSE; Benjamin et al. 2003; Churchwell et al. 2009). Based on these data, the source was included in the Spitzer/IRAC Candidate YSO (SPICY) catalogue (labelled SPICY 71482), where its spectral index $\alpha = -0.7$ suggests a Class II (disc-bearing) evolutionary stage (Kuhn et al. 2021a).

The 2022–2023 outburst was registered in the Gaia Alerts (Hodgkin et al. 2021) stream as Gaia22dtk (Hodgkin et al. 2022; Kuhn et al. 2022b) – the first recorded outburst from this source. The distinctiveness of this event in the source's light curve makes it a good case study for understanding accretion outbursts from later (post-embedded) evolutionary stages of YSOs.

In this study, we use photometry and spectroscopy to constrain the origin of the increased luminosity of the source as the outburst evolved. Section 2 describes the data. Section 3 examines the outburst light curve. Section 4 investigates the outburst spectra. Section 5 tracks the source's spectral evolution. Section 6 infers stellar properties. Section 7 characterizes the source's colour evolution. Section 8 discusses the astrophysical nature of the outbursting YSO. Finally, Section 9 provides our conclusions.

2 DATA AND OBSERVATIONS

The source's light curves and alert packets were obtained from time-domain photometric surveys, including the Zwicky Transient Facility (ZTF; Bellm et al. 2019; Graham et al. 2019), the Palomar Gattini-Infrared survey (PGIR; De et al. 2020), Gaia (Gaia Collaboration 2016; Hodgkin et al. 2021), the Visible and Infrared Survey Telescope for Astronomy (VISTA) Variables in the Vía Láctea (VVV; Minniti et al. 2010), and NEOWISE (Mainzer et al. 2011). Other photometry was obtained from VPHAS + (Drew et al. 2014), Pan-STARRS (Chambers et al. 2016; Flewelling et al. 2020), SDSS DR12 (Alam et al. 2015), DENIS (Fouqué et al. 2000), 2MASS (Skrutskie et al. 2006), UKIDSS (Lawrence et al. 2007; Lucas et al. 2008), GLIMPSE, and MIPS GAL (Carey et al. 2009; Gutermuth & Heyer 2015) surveys. Finally, the source was monitored during its 2023 dimming by the American Association of Variable Star Observers (AAVSO) using the 20-inch Telescope Altiplano de Granada (TAGRA) in Spain in Bessel and Sloan/SDSS bands. In the light curves assembled from this photometry (Fig. 1), the typical optical photometric error bars are smaller than the symbol sizes. For example, typical ZTF uncertainties were ≤ 0.05 mag in g and ≤ 0.02 mag in r . In the infrared, PGIR J -band uncertainties were ~ 0.25 mag during the outburst, but they were significantly larger when the source was near the detection threshold before brightening. In contrast, the median VVV JHK_s uncertainties were each < 0.03 mag, providing good constraints on the pre-outburst brightness. Uncertainties on the NEOWISE photometry were ~ 0.08 and ~ 0.05 mag for W1 and W2, respectively.

Spectroscopic follow-up in the optical and near-infrared was obtained whilst the source was near maximum brightness, during the decay, and after its return to quiescence. These observations (Table 1) were made with SpeX (Rayner et al. 2003) from NASA's Infrared

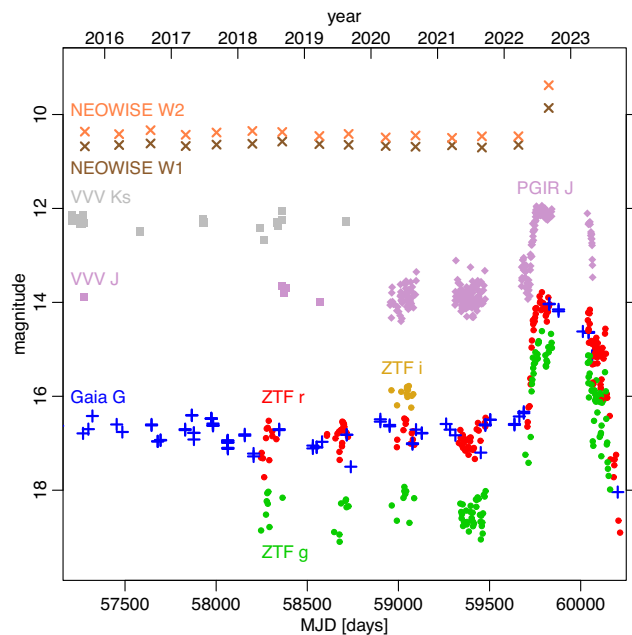


Figure 1. Optical and infrared light curves for V1741 Sgr over an ~ 8 yr period from 2015 to mid-2023. The light curves come from Gaia, ZTF, PGIR, VVV, and NEOWISE, and for MJD > 60000 , the ZTF photometry has been supplemented by AAVSO measurements. Most error bars are smaller than the symbols, so they are not depicted.

Telescope Facility (IRTF), the Low Resolution Imaging Spectrometer (LRIS; Oke et al. 1995) on Keck I, the Kast spectrograph (Miller & Stone 1993) on Lick Observatory's 3-metre Shane Telescope, and the Triple Spectrograph (TripleSpec; Herter et al. 2008) on Palomar Observatory's 200-inch Hale Telescope. SpeX and TripleSpec data were reduced with Spextools (Cushing, Vacca & Rayner 2004), LRIS with custom Interactive Data Language (IDL) scripts, and Kast with PyeIt v1.13.0 (Prochaska et al. 2020; Prochaska et al. 2023).

The LRIS and SpeX spectra, taken three days apart, overlap in the Z and Y bands. The shapes of the observed continua are consistent in this region. However, there is a factor of ~ 1.6 discrepancy between the recorded fluxes in the LRIS (higher) and SpeX (lower) spectra. This shift could represent source variability but could alternatively be attributed to light lost from the slit or uncertainty in absolute flux calibration. However, there is no extended emission around the source that could cause this discrepancy when the slit sizes differ. Given that this offset can cause difficulties in analysis, we scaled the spectra to match in the overlap region and used the closest-in-time PGIR measurement ($J = 12$ mag measured 27 days earlier) for absolute calibration. We apply scale factors of 0.9 to LRIS and 1.44 to SpeX to bring them into agreement. In the LRIS spectrum, the $\lambda 8662$ Ca II line is affected by a bad pixel, so we measured the Ca triplet lines from SpeX instead.

3 THE OUTBURST

The Gaia alert, Gaia22dtk, was based on a 2022 September 5 Gaia G -band measurement showing V1741 Sgr brighter than its historical level by 2.7 mag (Hodgkin et al. 2021, 2022).² The rise also triggered multiple alerts from the ZTF (ZTF18abfogsw) and Gattini (PGIR22agkate) surveys.

¹V1741 Sgr is entry #1 in the table of variable stars from Walker (1957) based on observations from the 20-inch Palomar reflector. However, it lies outside the field of view of Herbig's grating plates, so it was not assigned a LkH α number.

²<http://gsaweb.ast.cam.ac.uk/alerts/alert/Gaia22dtk/>

Table 1. Spectroscopic follow-up log.

Date	MJD [†]	Instrument	Facility	Exp s	Airmass	Slit "	Wavelengths Å	<i>R</i>	Standard	PI	Stage
(1)	(2)	(3)	(4)	(5)	(6)	(7)	(8)	(9)	(10)	(11)	(12)
2022 October 15	59868.2	SpeX	IRTF	720	1.7	0.5	7000–25 000	~2000	HD 159 415	M. Connelley	Peak
2022 October 18	59871.2	LRIS-blue	Keck I	300	1.6	1.0	3100–5650	~900	G191-B2B	C. Fremling	Peak
2022 October 18	59871.2	LRIS-red	Keck I	300	1.6	1.0	5650–10 200	~900	BD + 28 4211	C. Fremling	Peak
2023 April 24	60058.5	Kast-blue	Shane	650	2.1	1.5	3600–5500	~1100	Feige 34	R. M. Rich	Decay
2023 April 24	60058.5	Kast-red	Shane	310	2.1	1.5	5300–10 300	~1750	Feige 34	R. M. Rich	Decay
2023 August 5	60162.2	TripleSpec	P200	150	1.9	1.0	10 500–24 500	~2600	HD 157 734	C. Fremling	Quiesc.
2023 August 18	60175.2	Kast-blue	Shane	1600	2.1	1.5	3600–5500	~1100	P330E	R. M. Rich	Quiesc.

[†] Modified Julian day (MJD) is defined as heliocentric Julian day (HJD) minus 2400000.5.

(The reduced spectra are provided online as supplementary material.)

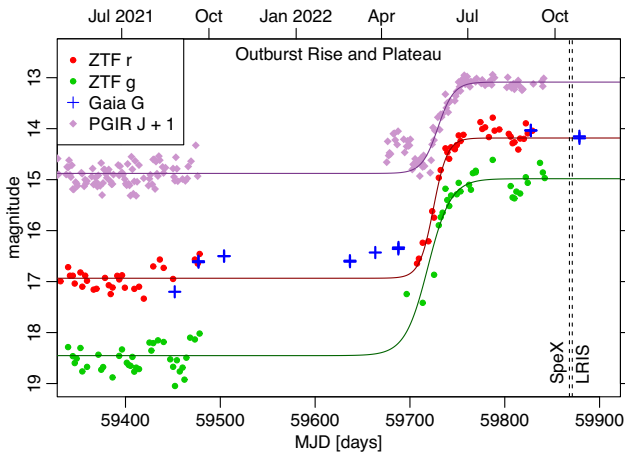


Figure 2. Zoom-in on the outburst rise as seen in the ZTF *g* and *r*-bands, the Gaia *G*-band, and the PGIR *J*-band. Logistic functions are fit to the ZTF data (red and green curves) and the combined VVV (not shown) plus PGIR data (purple curve). The vertical dashed lines indicate the dates of the first two spectroscopic observations.

The outburst’s rise occurred during early-to-mid 2022, and was detected in the Gaia *G*-band, ZTF’s *g* and *r*-bands, the PGIR *J*-band, and WISE’s *W1* and *W2* bands (Figs 1 and 2). In the Gaia light curve, the source brightened from a historical level of $G \sim 16.8$ mag to its alert magnitude of $G = 14.0$ mag, the brightest Gaia measurement to date. The last pre-outburst Gaia measurement was made on 2022 April 18, with $G = 16.3$ mag, which is close to the historical mean, indicating that most of the rise occurred between mid-April and early-September of that year. ZTF recorded the source brightening from $g \sim 18.4$ to 15.0 mag ($\Delta g \sim 3.4$ mag) and $r \sim 16.9$ to 14.2 mag ($\Delta r \sim 2.7$ mag), VVV + PGIR recorded the source brightening from $J \sim 13.8$ to 12.0 mag ($\Delta J \sim 1.8$ mag), and NEOWISE recorded the source brightening from $W1 \sim 10.6$ to 9.9 mag ($\Delta W1 \sim 0.8$ mag) and $W2 \sim 10.4$ to 9.4 mag ($\Delta W2 \sim 1.0$ mag). The brightening at visible wavelengths exceeds the factor-of-10 flux increase typically used as a threshold to classify events as outbursts (Fischer et al. 2023). Larger amplitudes at shorter wavelengths match expectations for YSO outbursts (Hillenbrand & Rodriguez 2022).

PGIR’s observability windows start slightly earlier than ZTF, providing finer detail about the initiation of the outburst (Fig. 2). This light curve showed a temporary ~ 1 mag brightening in April 2022, just before the start of the main rise.

Once V1741 Sgr reached maximum brightness in mid-July 2022, the light curve plateaued, lasting until the source became unobserv-

able from Palomar for several months during the winter season. There was a temporary ~ 0.5 mag dip in August 2022.

The decay of the outburst was captured during the spring and summer of 2023, when it faded from near-peak brightness to fainter than its pre-outburst state (Fig. 3). The first infrared and optical observations of 2023 came in April, with the source still in its plateau phase but showing some variability and a slight decline from the previous summer. However, by the end of that month, the decay had definitively begun. The next three months showed both dimming and rebrightening events, but the source finally reached its pre-outburst magnitude in August 2023 and dipped below this threshold in the subsequent months.

The history of monitoring V1741 Sgr extends back to 2015 for Gaia and 2010 for VVV and (NEO)WISE, but no previous burst or outburst was detected.

3.1 Modelling the rise

ZTF and PGIR sampled the light curve at multiple epochs along the entirety of the rise, revealing sigmoid-like behaviour (Fig. 2). The logistic curve,

$$m(t) = m_0 - \Delta m (1 + \exp((t - t_0)/\tau))^{-1}, \quad (1)$$

provides a convenient functional form to model the observed rises (e.g. Hillenbrand et al. 2018). Here, m_0 is the quiescent magnitude, Δm is the change in magnitude, t_0 is the time of the midpoint of the rise in MJD, and τ sets the rise time-scale. In the *r*-band, which is the best sampled, the middle of the rise occurs at $t_0 = 59724.8 \pm 0.9$ d (25 May 2022), and the rise has a timescale of $\tau = 7.3 \pm 0.8$ d. This time-scale indicates that ~ 90 per cent of the rise occurred in 2 months, with a maximum rise rate of $dm/dt = -0.094$ mag d⁻¹ for the fitted curve. For the *g*-band, $t_0 = 59718.9 \pm 1.8$ d and $\tau = 12.1 \pm 1.5$ d. To fit the *J* band, we used previous VVV measurements to constrain the pre-outburst magnitude and PGIR measurements for the outburst, finding $t_0 = 59731.2 \pm 1.5$ d and $\tau = 8.4 \pm 1.4$ d.

These fits indicate that the *g*, *r*, and *J* light curves were not synchronized but showed wavelength-dependent lags in when they reached their mid-points. The *g*-band light curve reached its mid-point first, followed by the *r*-band light curve with a delay of 6 d, and finally, the *J*-band light curve 6 d after that. These delays can be seen with visual inspection of Fig. 2, are statistically significant, and are similar to the τ brightening timescales. Each of the logistic-function fits is baselined to the long-term low-state of the light curves from ZTF or VVV, so these differences are not produced by slight differences in the optical and near-infrared observing seasons.

In the NEOWISE light curve, sampled every six months, only the last epoch (MJD 59824) showed significant brightening. This

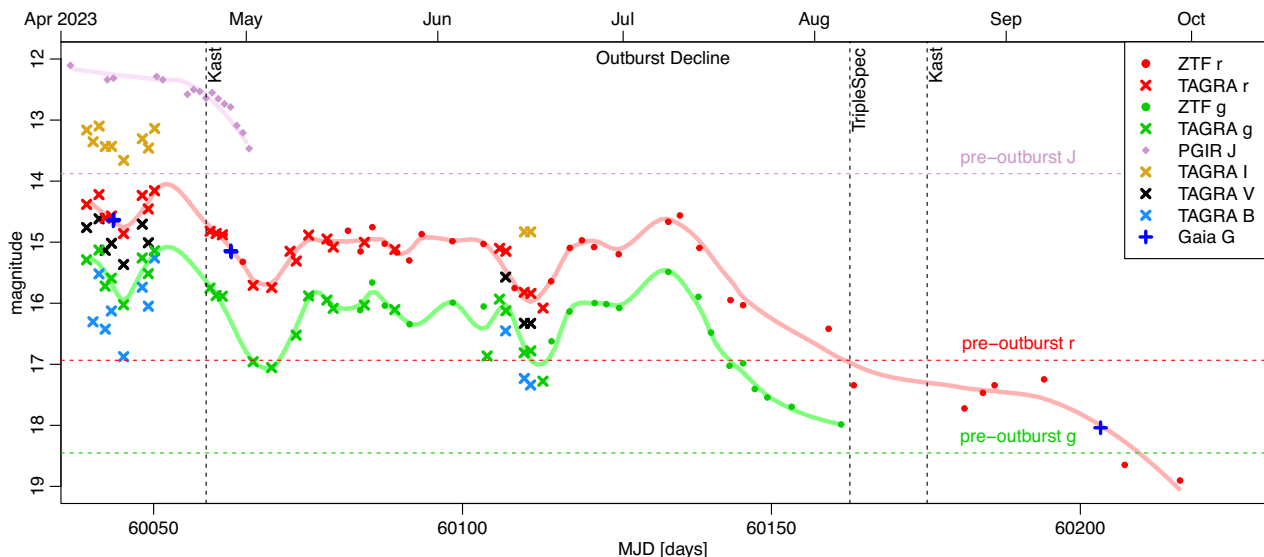


Figure 3. Multi-band light curves for V1741 Sgr during the Spring and Summer of 2023 while the source was dimming. Photometry include the PGIR J band, the ZTF g and r bands, the Gaia G band, and the TAGRA measurements in the Johnson-Cousins B , V , and I_c bands and the Sloan/SDSS g and r bands. Smoothed curves (loess regression) for the g , r , and J light curves are provided to guide the eye. Formal photometric uncertainties are smaller than the symbols, so error bars are not shown. Dates of spectroscopic observations are indicated by the vertical dashed lines, and the pre-outburst mean magnitudes are indicated by the horizontal dashed lines.

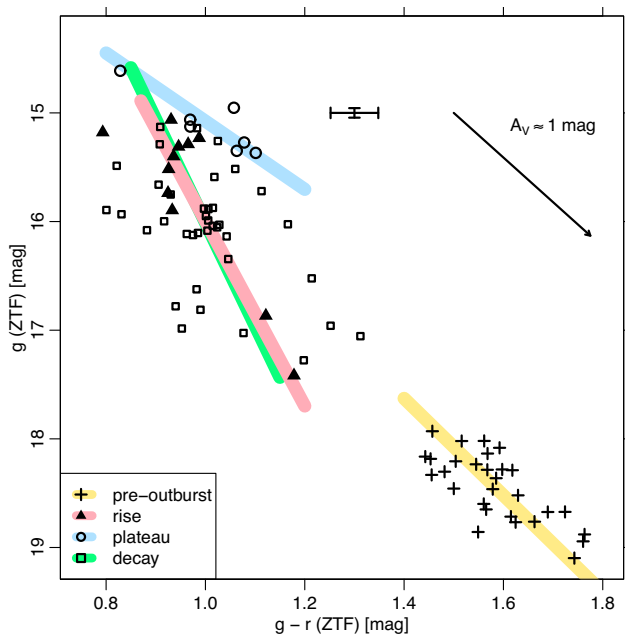


Figure 4. ZTF colour–magnitude diagram for the light curve’s pre-outburst, rise, plateau, and decay phases. Typical error bars and an $A_V \approx 1$ mag reddening vector bar are shown. The thick coloured lines show the orthogonal distance regressions for each phase of the light curve.

timing is consistent with the optical/near-infrared outburst (Fig. 1) and indicates that V1741 Sgr did not brighten in the mid-infrared pre-outburst.

3.2 Outburst decay

The shape of the g and r -band light curves during the decay do not mirror the rise, but instead, they are choppy with multiple dimming

and rebrightening events amidst a net decline (Fig. 3). Consequently, the sigmoid-like models from Section 3.1 do not describe these curves well. Once dimming began, the time for the source to reach its pre-outburst flux was ~ 110 d (~ 3.6 months), with a mean rate of $dr/dt = 0.025$ mag d^{-1} . This implies that the dimming phase of this outburst was slightly slower than the rising phase.

Local minima in the decay light curve are found at MJD 60045, 60067, and 60111. During the first of these, the light curve faded to near its pre-outburst magnitude in the J band. During a local maximum at MJD 60135, the source recovered much of its lost flux, before beginning a final rapid dimming.

In the final measurements before our cut-off date, the source became fainter than the pre-outburst level by $\Delta r \approx 2$ mag. This extra dimming was detected in one Gaia measurement and two r -band ZTF measurements. No previous dip of this depth had been recorded in monitoring of this source, suggesting that the dimming could have been triggered by the outburst.

3.3 Optical colour changes

Overall, bluer $g - r$ colours are correlated with brighter g -band magnitudes (Fig. 4). This behaviour is common for variable YSOs, where it can be explained by changes in extinction or accretion flows (e.g. Bouvier et al. 2003; Wolk et al. 2018; Hillenbrand et al. 2022b). The Cardelli, Clayton & Mathis (1989) extinction law with $R_V = 3.1$ yields the reddening relation³ $E(g - r) \approx 0.275A_V$ and $A_g \approx 1.13A_V$.

To analyse the colour variability of V1741 Sgr, we subdivided the light curves into phases, including pre-outburst (MJD 58200–59600), rise (MJD 59600–59777), plateau (MJD 59777–59850), and decay (MJD 60030–60170). To calculate colours, we matched ZTF g and r -band observations made within 12 h of each other.

³As this relation depends slightly on the source (e.g. Sale et al. 2009), we assumed a K-type stellar spectrum when calculating approximate reddening coefficients for the ZTF filters.

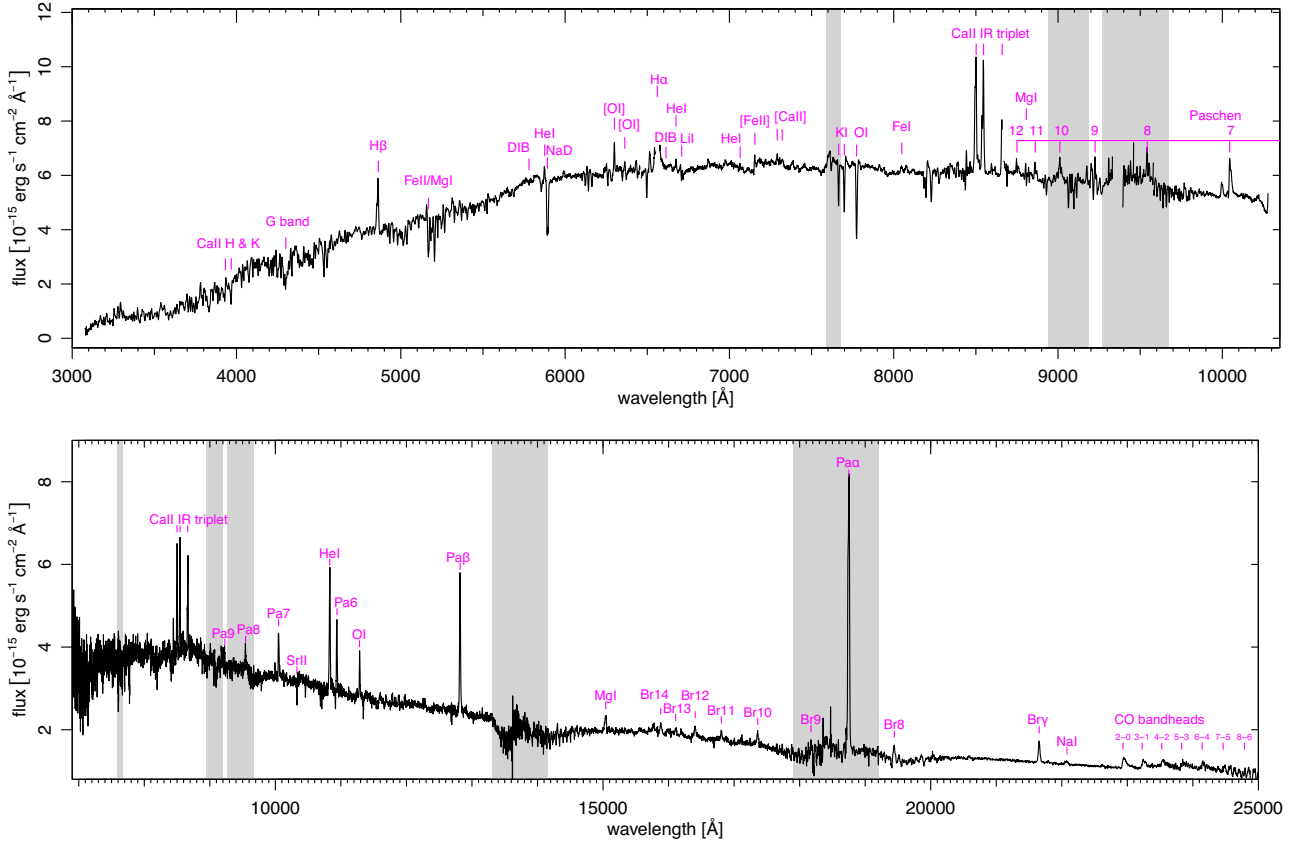


Figure 5. Spectra of V1741 Sgr during the outburst plateau from Keck/LRIS (top) and IRTF/SpeX (bottom). Prominent features are indicated. These spectra are shown as they appear in the original data, without the scaling described in Section 2. In both panels, spectroscopic regions affected by strong atmospheric absorption are shaded grey.

Regression lines are fit to the g versus $g - r$ data points in each phase of the light curve. We used the orthogonal distance regression (Golub & Van Loan 1980), implemented in the CRAN package *pracma* (Borchers 2022). This regression algorithm is well-suited for analysing these diagrams because it treats both colour and magnitude in a symmetric manner (Poppenhaeger et al. 2015; Hillenbrand et al. 2022b).

Whilst in its pre-outburst state, V1741 Sgr exhibited significant variability, with standard deviations of 0.3 mag in g and 0.25 mag in r . The slope for this phase, $\Delta g/\Delta(g - r) = 4.5 \pm 0.8$ (yellow line), is consistent with the reddening vector (slope = 4.1), suggesting that this variability may be attributed to extinction by circumstellar material.

At the start of the outburst, the source initially became bluer by $\Delta(g - r) = 0.4$ mag, but then, during the rise phase, the source’s brightness increased dramatically, with relatively little colour change. For this phase, the slope is 8.5 ± 1.2 (red line), significantly steeper than the reddening vector, implying that this brightness change is driven by something other than extinction. The initial blueward colour shift is connected to the ~ 6 -d lag between the g and r -band rises.

During the plateau, the slope of 3.1 ± 1.0 (blue line) is again consistent with variability produced by changes in extinction. Thus, the temporary dip in mid-August may have been an extinction-related event.

The slope during the decline is 9.5 ± 3.0 (green line), similar to that of the rise. However, there is considerably more scatter in the

versus $g - r$ diagram than during the earlier stages of the light curve. The width of the distribution is statistically significant, which may suggest that multiple phenomena contribute to the colour changes, possibly both extinction and accretion changes.

4 SPECTROSCOPY OF THE OUTBURST PEAK

At the outburst peak, the LRIS and SpeX spectra reveal a source with both emission and absorption features (Fig. 5). The strongest emission lines include the hydrogen Balmer, Paschen, and Brackett series, the Ca II infrared triplet (the Ca II H and K lines are not unambiguously detected), and He I lines (Table 2). Other emission lines include Fe I and Mg I, the Na I doublet at $\lambda\lambda 2.206/2.209 \mu\text{m}$, and forbidden [O I], [N II], [Ca II], and [Fe II] lines. The CO overtone bands are also detected in emission. In the optical, the spectrum is fairly red as a consequence of extinction (Section 4.3). However, in the near-infrared, the source has a blue continuum.

The strong emission lines, and especially the CO emission, indicate that the outburst from V1741 Sgr best fits into the EX Lup category (Fischer et al. 2023). The Li I $\lambda 6707$ absorption line is measured⁴ in the LRIS spectrum with an equivalent width of $W_\lambda =$

⁴To correct for blending with the nearby iron line, we use the relation from Jeffries et al. (2023) to estimate the contribution from $\lambda 6707.44$ Fe I for a stellar atmosphere with $T_{\text{eff}} \approx 4750$ K (Section 4.1). The expected contribution of 0.02 \AA is much smaller than the observed equivalent width.

Table 2. Emission lines (outburst state).

Line	λ Å	W_λ Å	f_{obs} erg s ⁻¹ cm ⁻² 10 ⁻¹⁵	L_{line} erg s ⁻¹ 10 ³⁰
(1)	(2)	(3)	(4)	(5)
H β	4861	-5.01 ± 0.25	17.9 ± 0.9	15 ± 6
He I	5876	-0.64 ± 0.03	3.3 ± 0.2	2 ± 1
[O I]	6300	-0.96 ± 0.01	5.3 ± 0.1	3 ± 1
O I	8446	-1.73 ± 0.19	9.4 ± 1.0	4 ± 1
Ca II	8498	-7.82 ± 0.27	43.3 ± 1.5	16 ± 3
Ca II	8542	-8.03 ± 0.26	44.7 ± 1.5	17 ± 3
Ca II	8662	-6.88 ± 0.25	38.8 ± 1.4	14 ± 2
Pa9	9230	-2.03 ± 0.09	9.9 ± 0.5	3 ± 1
Pa8	9546	-2.16 ± 0.19	10.9 ± 0.9	4 ± 1
Pa7	10049	-4.81 ± 0.12	22.8 ± 0.6	7 ± 1
He I	10830	-16.78 ± 0.29	72.2 ± 1.2	22 ± 3
Pa6	10938	-7.91 ± 0.24	33.9 ± 1.0	10 ± 1
O I	11287	-4.46 ± 0.15	18.1 ± 0.6	5 ± 1
Pa β	12818	-24.60 ± 0.29	86.9 ± 1.0	23 ± 2
Mg I	15040	-6.23 ± 0.17	17.6 ± 0.5	4.4 ± 0.3
Pa α	18751	-134.02 ± 0.96	284.0 ± 2.0	65 ± 3
Br γ	21661	-13.10 ± 0.24	22.9 ± 0.4	5.0 ± 0.2
Na I	22080	-3.48 ± 0.21	5.8 ± 0.4	1.3 ± 0.1

Columns 1–2: Spectral line identity. Below 20 000 Å, wavelengths are given in air and, above, in vacuum. Column 3: Equivalent width. Column 4: Observed line flux. Column 5: Extinction-corrected line luminosity assuming $A_V = 1.4 \pm 0.4$ mag and $\varpi = 0.795$ mas.

0.28 ± 0.03 Å, providing further evidence that V1741 Sgr is a young star.

Within the EX Lup category, there is significant diversity in spectroscopic features, both in terms of which features are present and the strengths of these features. To illuminate similarities and differences within this class, in Figs 6–7, we compare our spectra of V1741 Sgr to two other outbursting YSOs, the Class I source Gaia 19ajj with a 5.5 mag rise over 3 yr (Hillenbrand et al. 2019a) and the intermediate-mass star LkH α 225 S with a 7 mag rise over 15 yr (Magakian et al. 2019; Hillenbrand et al. 2022a).

4.1 Optical/near-infrared LRIS spectrum

In the optical spectrum (Fig. 5, top), absorption features resemble those of a K or G-type star, including the presence of the Fraunhofer G band (Gray & Corbally 2009). We modelled the normalized spectrum between 4000 and 4500 Å, masking out the H γ and H δ lines, using the BOSZ (Bohlin et al. 2017) stellar atmospheres plus a constant component to approximate the effect of veiling on spectral lines and assuming Solar metallicity. A 4750 K stellar atmosphere with a veiling component ~ 1.4 times the continuum level provided the best fit. However, the degeneracy between temperature and veiling, with higher veiling yielding lower temperatures, means these parameters are not well constrained.

Several lines present deeper absorption than a normal stellar photosphere, including the Mg I b triplet, the Na I D doublet, the $\lambda 7665$ and $\lambda 7699$ K I lines, and the $\lambda \lambda 7774$ O I triplet. These lines are frequently associated with winds in YSO spectra (e.g. Covey et al. 2011; Hillenbrand et al. 2018, 2022a); however, the resolution of our V1741 Sgr spectrum is too low to discern the kinematics.

The spectrum of V1741 Sgr shows Ba II absorption lines at $\lambda 6142$ and $\lambda 6497$ (Fig. 6, top). These are signatures of low-gravity atmospheres, including the atmospheres of circumstellar discs, and

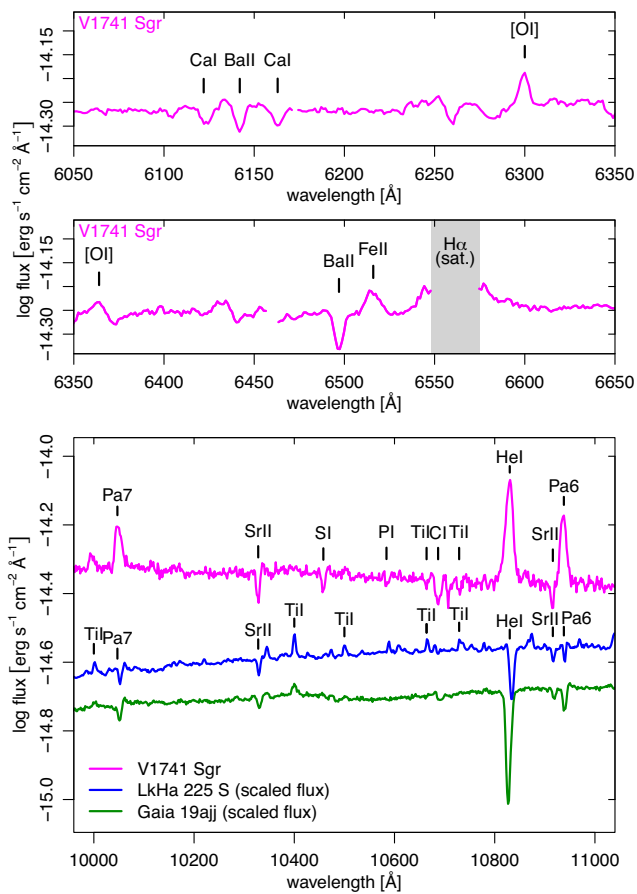


Figure 6. Detailed views of the outburst spectra in the r -band (top) and Y -band (bottom). In the bottom panel, SpeX spectra for Gaia 19ajj and LkH α 225 S are included for comparison.

are commonly observed in FU Ori-type stars (e.g. Reipurth 1990; Teodorani et al. 1997; Hillenbrand et al. 2019b).

4.2 Near-infrared SpeX spectrum

In the Y -band (Fig. 6, bottom), Sr II absorption lines provide further indication of low gravity. For F–M stars, the Sr II lines at $\lambda 1.0328$ μm and $\lambda 1.0916$ μm are strongest in supergiants, moderate in giants, and weak in dwarfs (Sharon et al. 2010; Hillenbrand et al. 2022a). These Sr II absorption lines are detected in V1741 Sgr, Gaia 19ajj, and LkH α 225 S, but they are strongest in V1741 Sgr.

The Y -band region of V1741 Sgr's spectrum exhibits atomic absorption lines with low-to-moderate excitation potentials, including the Sr II lines discussed above ($E_{\text{lower}} \sim 1.8$ eV), Ti I ($E_{\text{lower}} \sim 0.8$ eV), and C I, S I, and P I ($E_{\text{lower}} \sim 7$ eV). This region of the spectrum looks quite different for Gaia 19ajj or LkH α 225 S, where the Ti I lines are seen in emission and the C I, S I, and P I lines are not detected. The higher excitation C I, S I, and P I lines require temperatures of > 4700 K to form in stellar atmospheres (Sharon et al. 2010). For example, in their sample of standard stars, C I $\lambda 1.0688$ μm absorption is only detected from supergiants with $T_{\text{eff}} \gtrsim 4700$ K, giants with $T_{\text{eff}} \gtrsim 5100$ K, or dwarfs with $T_{\text{eff}} \gtrsim 5800$ K.

In the J band (Fig. 7, top left), outbursting YSOs often exhibit numerous emission lines between 1.150 μm and 1.210 μm from Fe I, Mg I, Si I, and K I (e.g. Kóspál et al. 2011; Hodapp et al. 2019).

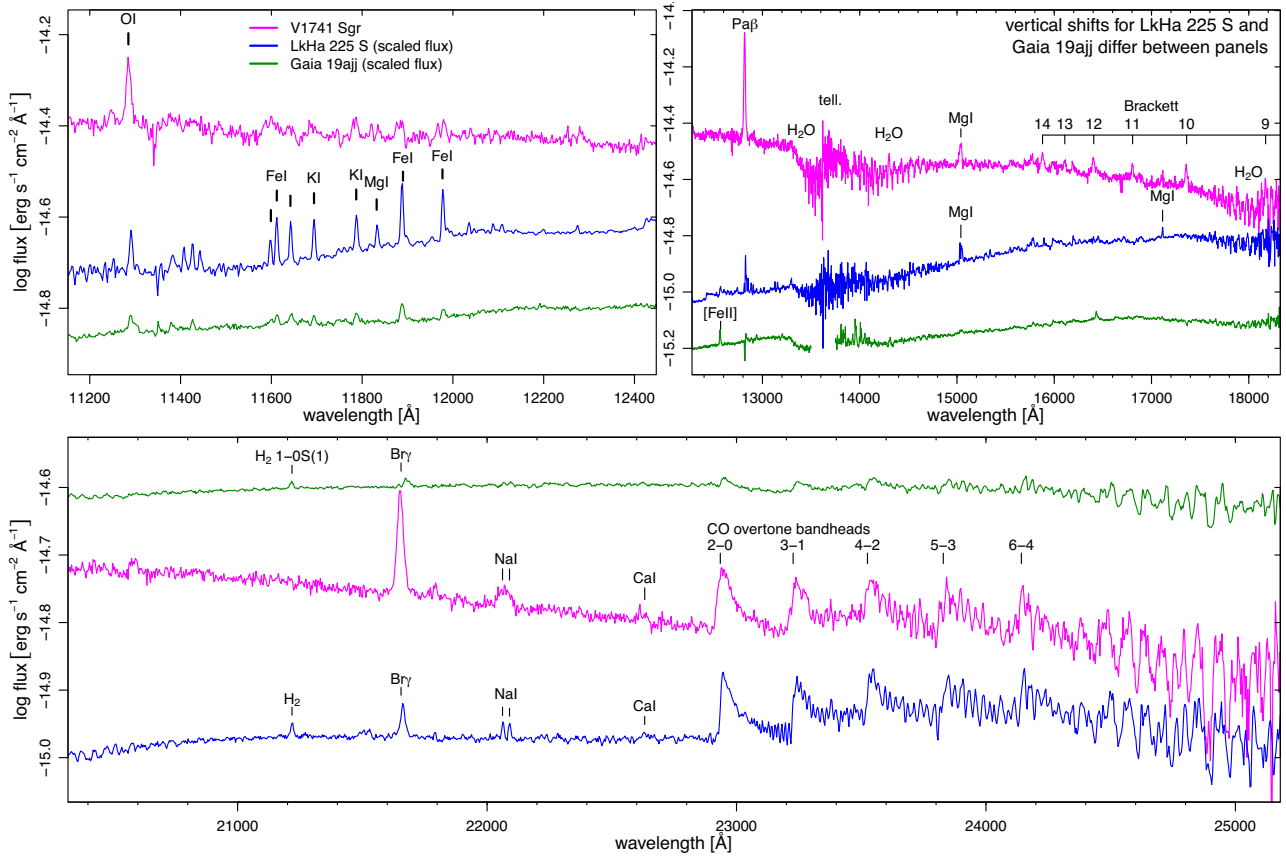


Figure 7. Detailed views of the outburst SpeX spectra for V1741 Sgr (magenta), LkH α 225 S (blue), and Gaia 19ajj (green) in spectral regions around the *J* (top left), *H* (top right), and *K* (bottom) bands.

These can be seen in the spectrum of LkH α 225 S, or, more weakly, in the spectrum of Gaia 19ajj (Hillenbrand et al. 2022a). However, these lines are much weaker in the spectrum of V1741 Sgr. In contrast, the nearby λ 1.1287 μ m O I line is relatively stronger in V1741 Sgr than in the other two spectra.

A sharp down-turn in the spectrum of V1741 Sgr around 1.34 μ m indicates the onset of water absorption, and absorption features can also be seen on both sides of the *H*-band spectrum (Fig. 7, top right). Similar absorption features were detected in the Gaia 19ajj and LkH α 225 S spectra (Hillenbrand et al. 2019a, 2022a), but the features are slightly weaker in those stars. Furthermore, the water absorption in each of these three stars is much weaker than the water absorption frequently seen in FU Ori stars, where the effect of low gravity can give the *H*-band a characteristic triangular shape (e.g. Connelley & Reipurth 2018). Water absorption is typically found in the spectra of M-type stars, becoming prominent at lower temperatures than molecular absorption from TiO and VO (Gray & Corbally 2009). However, no TiO or VO absorption was detected in the LRIS or SpeX V1741 Sgr spectra.

Spectra of EX Lup-type stars frequently exhibit H $_2$ emission associated with shocked gas in outflows (e.g. Guo et al. 2020; Giannini et al. 2022; Kóspál et al. 2023). However, no H $_2$ lines were detected in our spectrum of V1741 Sgr (Fig. 5, bottom), with an upper limit of $<4 \times 10^{-16}$ erg s $^{-1}$ cm $^{-2}$ on the strongest of these lines at λ 2.12 μ m. In contrast, the λ 2.12 μ m line was detected in the spectra of both LkH α 225 S and Gaia 19ajj, even while these stars were in outburst.

The Na I doublet at λ 2.206/2.209 μ m is detected as a blended emission line with an equivalent width of -3.45 Å. It is stronger in V1741 Sgr than in either Gaia 19ajj (not detected) or in LkH α 225 S (weakly detected), but similar to the strength of the Na I lines initially detected from EX Lup (-2.45 Å; Kóspál et al. 2011).

In V1741 Sgr, the CO overtone bands are strong emission features (Fig. 7, bottom), with a similar strength relative to the continuum as LkH α 225 S and much stronger than for Gaia 19ajj (Fig. 7, bottom). CO in emission is a common trait of EX Lup-type sources, whereas CO absorption is required in the definition of FU Ori-type stars (Connelley & Reipurth 2018). The strengths and profile shapes of the CO bands here resemble the outburst CO spectrum of EX Lup (Kóspál et al. 2011, their fig. 7), which was found to be well-described by CO emission from a 2500 K slab model.

4.3 Diffuse interstellar bands and extinction

The extinctions of outbursting stars are challenging to measure owing to the unknown spectrum of the underlying sources. However, diffuse interstellar bands (DIBs) can serve as extinction estimators that do not require knowledge of spectral shape. In the LRIS spectrum, the DIBs at λ 5780 and λ 6614 Å are detected with equivalent widths of 0.208 ± 0.024 and 0.072 ± 0.018 Å, respectively. Carvalho & Hillenbrand (2022) note that DIB absorption may be contaminated by Fe I, Cr I, Si I, and Sc II lines in stars with spectral types later than G0. In their sample of outbursting YSOs, they calculate that contamination may account for ~ 0 –50 per cent of the absorption in

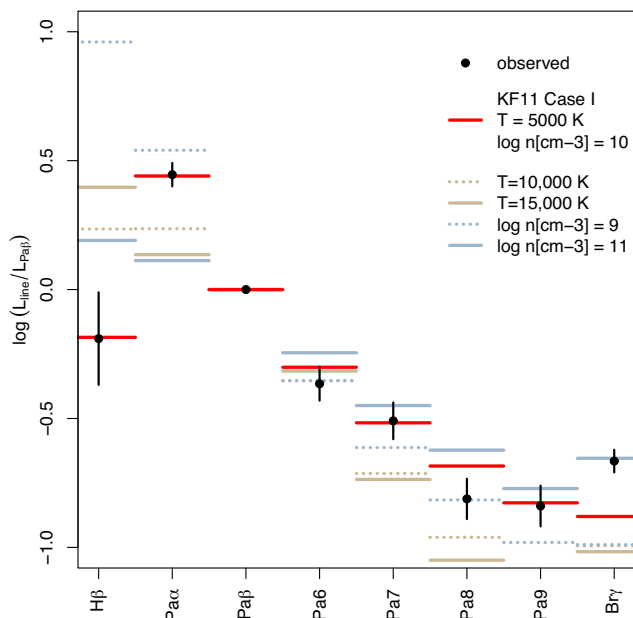


Figure 8. Ratio of the luminosities of various H lines to Pa β . The logarithmic line ratio is the ordinate, and the identity of the line in the numerator is the abscissa. The red lines indicate the ratios from the best-fitting model from Kwan & Fischer (2011) Case I. Other models with different temperatures or densities are included for comparison.

these features. Thus, the extinction values we calculate from these DIBs should be considered upper limits.

The relations between DIB equivalent widths and extinctions (Carvalho & Hillenbrand 2022, their equations 4 and 5) predict $E(B - V) = 0.45 \pm 0.12$ from the $\lambda 5780$ DIB or $E(B - V) = 0.35 \pm 0.11$ from the $\lambda 6614$ DIB. Assuming an extinction law with $R_V = 3.1$, these correspond to $A_V \sim 1.4$ mag or 1.1 mag, respectively.

Along the line of sight towards V1741 Sgr, the extinction estimated by the Bayestar (Green et al. 2019) map increases gradually up to a distance of ~ 1100 – 1200 pc, where extinction jumps by 0.6 mag from $A_V = 0.6$ mag to $A_V = 1.2$ mag, followed by another gradual increase at greater distances.⁵ This suggests the presence of a wispy local cloud in the vicinity of V1741 Sgr. Together with the DIB measurements, these results constrain V1741 Sgr's extinction during outburst to $A_V = 0.6$ – 1.4 mag. If V1741 Sgr is partially obscured by its local cloud, it likely lies near the upper end of this range.

4.4 H I, He I, Ca II, and O I emission lines

Hydrogen emission line ratios probe the conditions of the emitting gas. We compare emission lines to predictions for models of T Tauri stars with a photoionization rate of $\gamma_{\text{HI}} = 2 \times 10^{-4} \text{ s}^{-1}$ (Kwan & Fischer 2011).⁶ For this analysis, we used H emission lines with adequate signal to noise and computed the ratio of the extinction-corrected line luminosities to the Pa β line (Fig. 8). The best fit was provided by a model with a temperature of $T = 5000$ K and density of $\log n[\text{cm}^{-3}] = 10$. This fit accurately reproduces the ratio of H β to Paschen lines and the Paschen decrement. However, it underestimates the luminosity of the Br γ line by ~ 50 per cent. The good fit to the

Balmer and Paschen lines implies that the assumed extinction of $A_V \lesssim 1.4$ mag is reasonable. Modifying extinctions is insufficient to resolve the discrepancy for the Br γ line since the Pa α and Br γ lines are in the same spectral region and thus subject to similar extinctions.

Fig. 8 also compares the results to several alternative models. Models with higher temperatures overestimate H β and underestimate Pa α and Pa7–9. A model with ten times lower density overestimates the line strength of H β by more than dex. Finally, a model with ten times higher density provides a slightly worse fit to H β and the Paschen decrement than our best-fitting models but provides an improved fit to Br γ . Thus, it is possible that the discrepancy between the Br γ and our best-fit model could be explained if the Br γ emission was dominated by a slightly denser plasma. Fitting using the lower photoionization rate ($\gamma_{\text{HI}} = 2 \times 10^{-6} \text{ s}^{-1}$) models from Kwan & Fischer (2011) yielded similar results.

Our best-fitting density falls in the range found for other EX Lup-type stars observed in a high state, including XZ Tau, NY Ori, and PV Cep with $9 \lesssim \log n \lesssim 11$ (Giannini et al. 2022). However, the best-fitting temperature for V1741 Sgr lies at the lower end of the temperature range $5000 \text{ K} \lesssim T \lesssim 12\,500 \text{ K}$.

The Pa γ /He I $\lambda 10830$ ratio for V1741 Sgr is ~ 0.5 , which implies that the Pa γ line is moderately optically thick ($\tau_{\text{Pa}\gamma} \sim 0.8$) according to the models of Kwan & Fischer (2011, their fig. 8). The He I $\lambda 5876$ /He I $\lambda 10830$ ratio of ~ 0.06 , implies that the He I $\lambda 5876$ line is very optically thin and is lower than observed in the T Tauri stars examined by Kwan & Fischer (2011, their fig. 10). According to their models, these ratios constrain the temperature to 5000–15 000 K, consistent with the above values.

The Ca II infrared triplet lines are observed strongly in emission, with no absorption component. Their line ratios (obtained from the SpeX spectrum) are close to unity, implying that they are optically thick, with a peak intensity pattern $I_{\lambda 8542} > I_{\lambda 8498} > I_{\lambda 8662}$ that is fairly typical for T Tauri stars (Hamann & Persson 1992; Azevedo et al. 2006). In contrast, the Ca II H and K lines are not unambiguously detected despite sharing upper energy levels with the Ca II infrared triplet (Merrill 1943). A comparable scenario was observed in the outburst spectrum of LkH α 225 S, where both emission and absorption P Cygni components were observed for the Ca II infrared triplet, but Ca II H and K were only detected in absorption (Hillenbrand et al. 2022a). In the infrared, the Ca II triplet emission would be much stronger than the Ca II triplet absorption, so only the emission component is visible in V1741 Sgr's spectrum. Meanwhile, in the blue part of the spectrum, the absorption component is deeper, so it is only just filled by the emission component, leading to an absence of these lines. A similar scenario may explain the lack of Balmer lines blueward of H β .

The forbidden [Ca II] $\lambda 7291$ and $\lambda 7324$ transitions, whose upper state is the lower state of the permitted Ca II triplet (Merrill 1943), are detected weakly in emission by LRIS. These lines are fairly rare in YSOs but observed during some outbursts, including Gaia 19ajj and LkH α 225 S (Hillenbrand et al. 2019a, 2022a).

The O I $\lambda 8446$ and $\lambda 11287$ lines are sensitive to Ly β irradiation, which can excite ground-state O I to the $3d \ ^3D$ state, which may then de-excite via sequential emission of $\lambda 8446$, $\lambda 11287$, and $\lambda 1303$ photons (Bowen 1947; Kastner & Bhatia 1995). For V1741 Sgr, both of these O I emission lines are strong, with a $\lambda 11287/\lambda 8446$ flux ratio of 1.5, moderately larger than the ratio of photon energies. The $\lambda 8446/\text{Pa } \gamma$ ratio is 0.35, which yields a similar $\tau_{\text{Pa}\gamma} = 0.8$ as above (Kwan & Fischer 2011, their fig. 15). For comparison, both LkH α 225 S and Gaia 19ajj exhibit $\lambda 11287$ emission, but the $\lambda 8446$ line is in absorption in the former and not detected in the latter. Kwan & Fischer (2011) note that $\lambda 8446$ absorption can result from radiative

⁵Bayestar colours were converted to A_V following the recommended extinction law from Green et al. (2019).

⁶https://www.stsci.edu/~wfischer/line_models.html

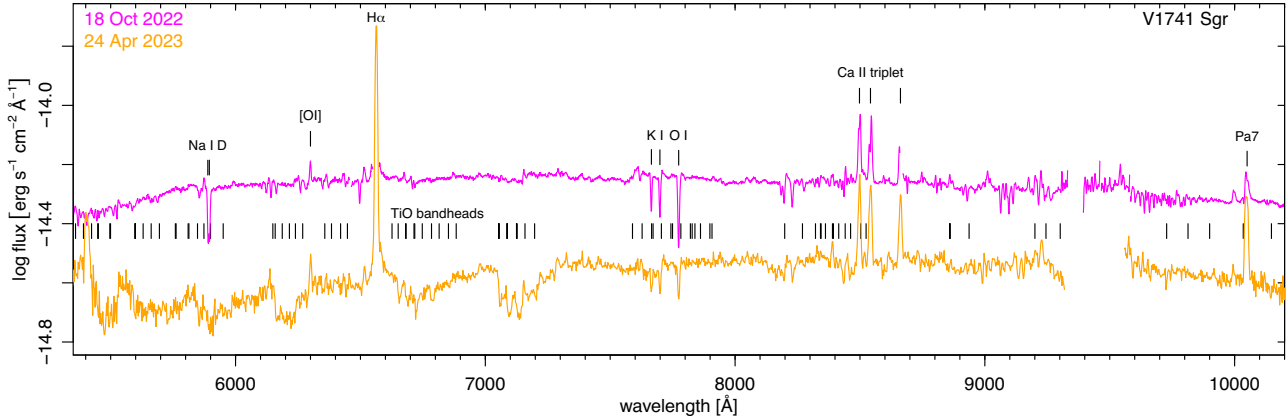


Figure 9. ‘Red’ side spectra during the outburst plateau (LRIS; 2022 October 18) and during the decline (Kast; 2023 April 24). Each spectrum is shown on an absolute, calibrated log-flux scale. Wavelengths of strong TiO bandheads are marked by the black ticks as indicated.

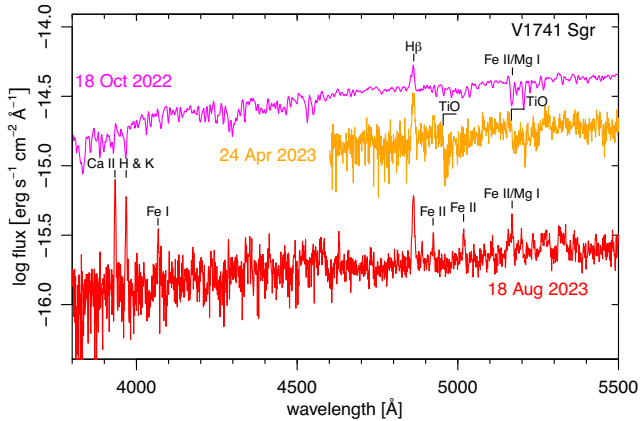


Figure 10. ‘Blue’ side spectra during the outburst plateau (LRIS; 2022 October 18), during the decline (Kast; 2023 April 24), and after return to quiescence (2023 August 18; Kast). Each spectrum is shown on an absolute, calibrated log-flux scale. Prominent lines and molecular bands are marked. A noisy region of the 2023 April 24 Shane/KAST spectrum, resulting from a shorter exposure time, is masked for visual clarity.

trapping of the $\lambda 1303$ photons, which may indicate optically thicker gas in those outbursters than in V1741 Sgr.

5 SPECTRAL EVOLUTION

Further monitoring of V1741 Sgr revealed spectroscopic changes to the source as it faded during the spring and summer of 2023. The first Shane/Kast spectra (2023 April 24) were taken after the source had declined about halfway from its peak. Nevertheless, even at this stage, the source was ~ 5 – 10 times brighter than its pre-outburst state, with its flux still dominated by the outburst. However, by the next Shane/Kast observation (18 Aug 2023), the source had returned to its pre-outburst flux. Only the blue-side Kast spectrum was obtained on this date. A post-outburst TripleSpec observation (2023 August 5) was also made around the same time.

The spectra in Figs 9–10 are presented with absolute flux calibration, revealing the decline in continuum flux over the full wavelength range with each subsequent spectrum.

5.1 Shane/Kast spectra of the decaying outburst

Between the LRIS observation and the first Shane/Kast observation, the absorption features dramatically changed, with TiO absorption becoming dominant as the source began to fade (Figs 9 and 10). In the blue-side Kast spectrum, TiO bands appeared, starting at 4954 and 5167 Å (part of the TiO α system). On the red side, the TiO absorption features were even clearer (owing to the better signal-to-noise), with strong features starting at 5759 Å (α system), 6149 Å (γ' system), 6651 Å, and 7045 Å (γ system).

The pattern of TiO band strengths, plus the lack of detected VO absorption, suggests an early M spectral type according to the classification scheme of Kirkpatrick, Henry & McCarthy (1991). The spectral indices from Herczeg & Hillenbrand (2014, their table 3) provide quantitative spectral type estimates. For the April 2023 spectrum, the index $x_{\text{TiO}7140} = -0.48$ indicates a spectral type of M1–M2 ($T \approx 3560$ – 3720 K). The level of veiling in the R band may be a source of systematic error on this estimate, with more veiling leading to earlier estimated spectral types (Fang et al. 2020).

Several wind-associated absorption features weakened or disappeared. For example, the equivalent widths of the $\lambda\lambda 7665/7699$ K I lines and the $\lambda 7774$ O I triplet decreased by a factor of ~ 0.8 and the Na I D doublet (blended with TiO) disappeared.

Conversely, the prominent emission lines do not weaken relative to the continuum but, in some cases, become stronger. Slight strengthening relative to the continuum is detected in H β , [O I], and the Ca II triplet, and significant strengthening is detected in Pa7. In absolute flux, all these lines dimmed somewhat, apart from Pa7, but not as rapidly as the overall dimming of the source.

5.2 Post-outburst spectra

The final Shane/Kast blue-side spectrum from August 2023 (Fig. 10) again revealed changes in spectroscopic features as the star continued to dim. The TiO absorption, seen in the previous Kast blue-side spectrum, is gone. The absence of these features implies a spectral type of K9 or earlier. Furthermore, the MgH band, detected in late K stars, is also not detected, implying a spectral type of K5 or earlier (Gray & Corbally 2009). Together, these constraints indicate a spectroscopic temperature of > 4140 K (Pecaut & Mamajek 2013), implying that the emission was dominated by hotter gas at this epoch than the previous one.

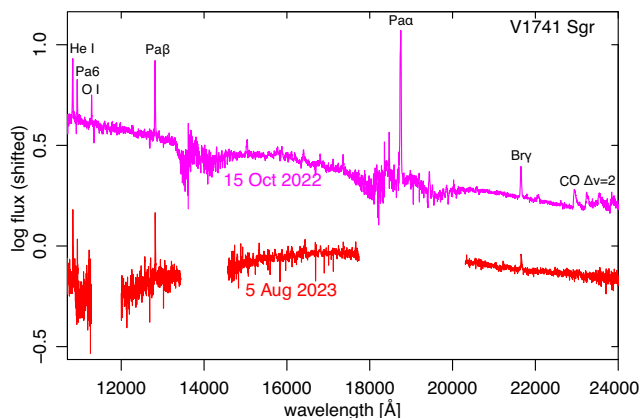


Figure 11. Near infrared spectra during the outburst plateau (SpeX; 2022 October 15) and after return to quiescence (TripleSpec; 2023 August 5). The TripleSpec spectrum does not have absolute flux calibration, so the relative vertical positioning of the spectra is arbitrary.

At this epoch, several emission lines appeared or strengthened. H β continued to strengthen relative to the continuum. Furthermore, strong emission was seen from the Ca II H and K lines, which were absent during the outburst. This spectrum also shows the appearance of iron emission lines, including $\lambda 4064$ Fe I, $\lambda 4924$ and $\lambda 5018$ Fe II, and the $\lambda 5169$ Fe II/Mg I blend, with the latter having transitioned from absorption to emission.

The near-infrared also presented changes in spectroscopic features between the outburst and post-outburst epochs (Fig. 11). Notably, emission was no longer detected from the CO bands, providing further evidence that the EX Lup-like outburst was over. H I and He I lines were still detected in this wavelength range, but the Pa β and longer-wavelength hydrogen lines became weaker relative to the continuum, opposite the behaviour of hydrogen lines at shorter wavelengths.

6 STELLAR PROPERTIES

The source of the outburst is likely a relatively isolated Classical T Tauri star, with a mass slightly less than our Sun and a relatively high quiescent accretion rate. The evidence for this characterization, inferred from pre-outburst data, is presented in the following section.

6.1 Lagoon nebula membership

V1741 Sgr is projected near the edge of the Lagoon Nebula, separated by $\sim 0.7^\circ$ from the main NGC 6350 cluster (Walker 1957). To verify whether this association is physical, we examined Gaia’s Early Data Release 3 (EDR3; Gaia Collaboration 2021), which provides a 6-parameter astrometric solution for V1741 Sgr (Lindgren et al. 2021a). Its parallax is $\varpi = 0.795 \pm 0.072$ mas, corrected for a zero-point offset of $z_p = -0.042$ mas (Lindgren et al. 2021b), which corresponds to a distance of ~ 1260 pc. Its proper motions are $\mu_{\alpha^*} = 1.360 \pm 0.076$ mas yr $^{-1}$ and $\mu_{\delta} = -1.213 \pm 0.056$ mas yr $^{-1}$ in equatorial coordinates, corresponding to $\mu_{\ell^*} = -0.379 \pm 0.061$ mas yr $^{-1}$ and $\mu_b = -1.789 \pm 0.0716$ mas yr $^{-1}$ in Galactic coordinates. The source’s renormalised unit weight error of 1.033 is close to unity, it has a small non-statistically significant astrometric excess noise of 0.22 mas, and 16 visibility periods were used.

The projected locations of YSOs in the neighbourhood of V1741 Sgr were obtained from the SPICY catalogue (Fig. 12). In this cata-

logue, candidate YSOs were identified solely from infrared photometry, employing spectral energy distribution (SED) fitting and statistical classification, meaning that these sources trace the distribution of star formation over a large swath of the Galactic midplane with minimal spatial bias (Kuhn et al. 2021a). In the vicinity of V1741 Sgr, three groups are detected:

(i) **G6.0-1.3** This is the main star cluster in the Lagoon Nebula, including stars from NGC 6530 and the Hour Glass Nebula. Its mean parallax is $\varpi = 0.821 \pm 0.006$ mas ($d = 1220_{-20}^{+30}$ pc), and its mean proper motions are $\mu_{\ell^*} = -1.18$ mas yr $^{-1}$ and $\mu_b = -2.19$ mas yr $^{-1}$ (Kuhn et al. 2021b).

(ii) **G5.9-0.9** This group is half a degree north-west of NGC 6530, but lies within the boundary of the Lagoon Nebula. Kuhn et al. (2021b) calculated a parallax of 0.774 ± 0.020 mas ($d = 1290 \pm 30$ pc) and proper motions of $\mu_{\ell^*,0} = -0.83$ mas yr $^{-1}$ and $\mu_{b,0} = 2.49$ mas yr $^{-1}$ that are statistically consistent with the other Lagoon Nebula members.

(iii) **G6.1-0.3** This group corresponds to RAFGL 2046. Its parallax, $\varpi_0 = 0.357 \pm 0.019$ mas (Kuhn et al. 2021b), places it behind Lagoon at a distance of 2800_{-140}^{+150} pc. Its mean proper motions are $\mu_{\ell^*,0} = -0.98$ mas yr $^{-1}$ and $\mu_{b,0} = -0.68$ mas yr $^{-1}$, with a b component significantly discrepant from the Lagoon Nebula.

V1741 Sgr is projected between the latter two groups. However, the star’s Gaia EDR3 parallax is most consistent with the Lagoon Nebula. We modelled the parallax–proper-motion distribution of the YSOs in this region with a mixture of Gaussians using the `mclust` software (Fraley & Raftery 2002; Scrucca et al. 2016). The best-fitting model included one component for the Lagoon Nebula stars (G6.0-1.3 and G5.9-0.9), another for RAFGL 2046 (G6.1-0.3), and a small non-clustered population of unassociated stars (Fig. 12, right). This model supports V1741 Sgr’s Lagoon membership (97 per cent probability), with a lower probability of non-association (3 per cent), and a negligible probability of RAFGL 2046 membership (< 0.001 per cent).

Within the Lagoon Nebula, the cluster NGC 6530 is expanding with an average outward velocity of ~ 1 km s $^{-1}$ (Kuhn et al. 2019; Wright et al. 2019). However, neither V1741 Sgr nor the nearby subcluster G5.9-0.9 are moving away from NGC 6530, as would be expected if they were to follow the same expansion pattern. This implies that these peripheral association members were not ejected from the central cluster but likely formed on the outskirts (see similar cases in Kuhn et al. 2022a, 2023b).

6.2 Quiescent YSO properties

V1741 Sgr’s pre-outburst SED suggests a reddened stellar photosphere with excess in the near-ultraviolet and mid-infrared bands (Fig. 13, top left). The time-averaged Gaia BP/RP spectrum for 2014–2017 (De Angeli et al. 2023; Montegriffo et al. 2023) shows a prominent H α emission line (Fig. 13, top right). These attributes are expected in the standard magnetospheric model of accreting T Tauri stars, where accretion luminosity provides the ultraviolet excess, disc emission provides the infrared excess, and H α emission is largely attributed to irradiated gas in accretion streams or winds (Hartmann, Herczeg & Calvet 2016).

To constrain the star’s effective temperature (T_{eff}) and V-band extinction (A_V), we fit the SED with BOSZ stellar atmosphere models (Bohlin et al. 2017) reddened by the Cardelli, Clayton & Mathis (1989) extinction law in the optical/near-infrared and the Wang, Li & Jiang (2015) law in the mid-infrared. The models were convolved

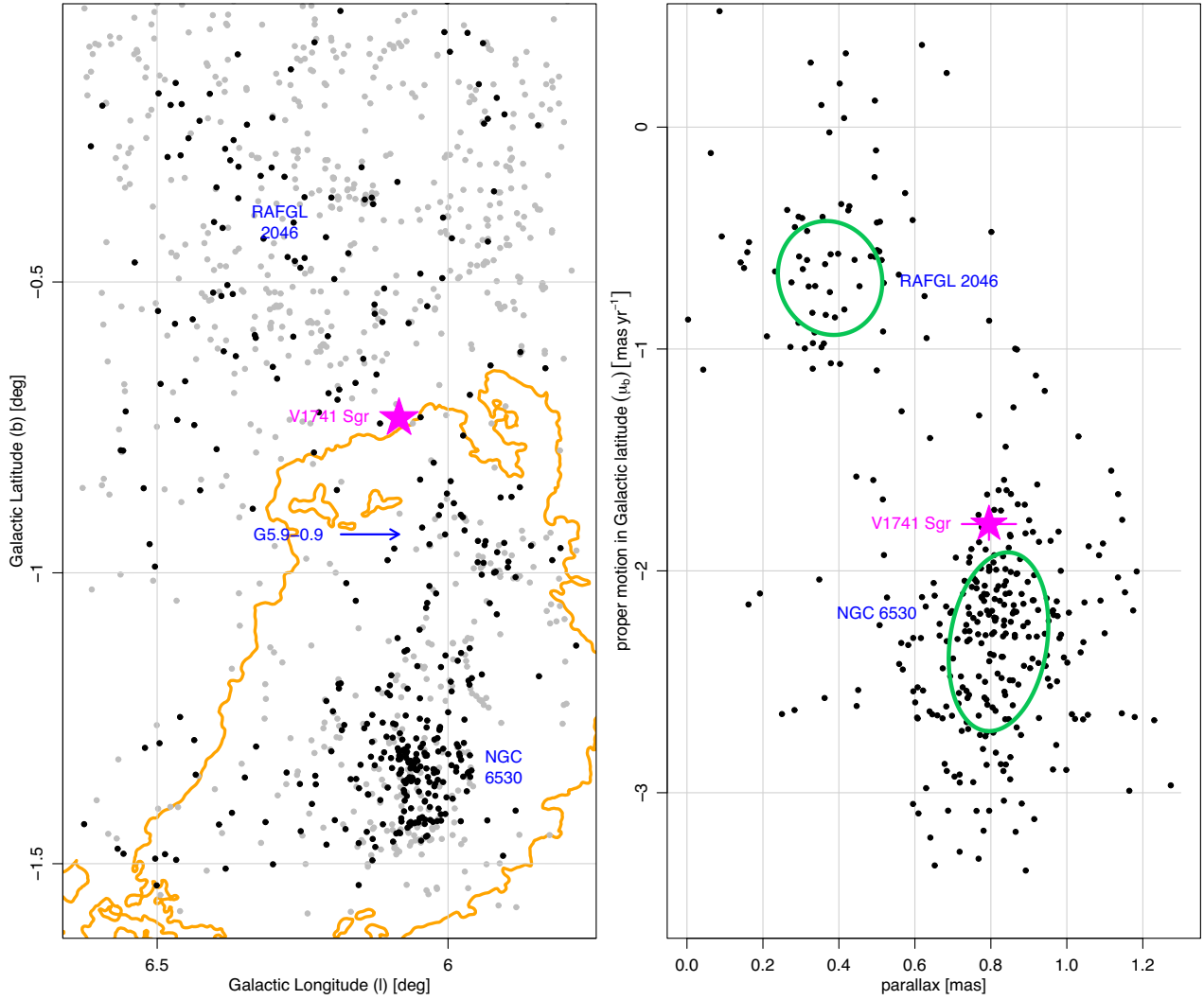


Figure 12. Left: Spatial distribution of YSOs in the neighbourhood of V1741 Sgr. YSOs with good Gaia astrometry are black points, those without are grey points, and V1741 Sgr is the magenta star. The three nearby YSO groups are labelled in blue. The optical nebulosity from the Lagoon Nebula is outlined with the orange contours derived from the Digitized Sky Survey red-band image (Lasker et al. 1990). Right: Astrometry for V1741 Sgr (magenta star) and neighbouring YSOs (black points). The green ellipses mark the two Gaussian mixture-model components found in parallax–proper-motion space, one corresponding to the Lagoon Nebula and the other to RAFGL 2046. V1741 Sgr’s astrometry is most consistent with the former.

with filter profiles obtained from the Spanish Virtual Observatory⁷ (Rodrigo, Solano & Bayo 2012; Rodrigo & Solano 2020) to predict flux in individual photometric bands. Our statistical model includes normally distributed photometric measurement errors (σ_{phot}) and an additional normally distributed error term (σ_{ε}) to account for astrophysical scatter (e.g. stellar variability). Only photometric measurements without blue or infrared excess (i.e. those between 4600 and 22 000 Å) were included in the fit. The log-likelihood function was maximised using the BFGS algorithm (Broyden 1970; Fletcher 1970; Goldfarb 1970; Shanno 1970) implemented by the *R* function `optim` (R Core Team 2022). To calculate Bayesian posterior distributions, we assumed uniform priors for all parameters, with $3500 \leq T_{\text{eff}} \leq 10,000$ K, $0 \leq A_V \leq 10$, $-10 \leq \log \sigma_{\varepsilon} \leq 10$, and $-100 \leq \log \text{scale} \leq 0$.

⁷<http://svo2.cab.inta-csic.es/theory/fps/>

The maximum likelihood T_{eff} is 4380 K, which is consistent with the constraints from the post-outburst spectrum (Section 5.2). However, the posterior distribution has a heavy tail extending to higher temperatures, meaning that higher temperatures cannot be absolutely excluded (Fig. 13, bottom left). The 1σ (68 per cent) credible interval is 4100–5850 K (i.e. spectral types K6–G2), whilst the 95 per cent credible interval is 3850–8200 K. Assuming a temperature of 4380 K, the corresponding extinction would be $A_V = 2.6 \pm 0.2$ mag. However, there is considerable degeneracy between A_V and T_{eff} (Fig. 13, bottom right). Nevertheless, the models yield a lower limit of $A_V > 1.5$ mag, with possible extinctions extending to 5.5 mag for the highest temperature models. The $T_{\text{eff}} = 4380$ K solution corresponds to a star with a luminosity (excluding contributions from accretion or disc emission) of $\log(L_*/L_{\odot}) = 0.35 \pm 0.20$ and a radius of $R_* = 2.6 \pm 0.3 R_{\odot}$. (The full range of possible luminosities are indicated on Fig. 14.)

Our best-estimate pre-outburst A_V of 2.6 mag is higher than the best-estimate $A_V \approx 1.4$ mag during the outburst (Section 4.3),

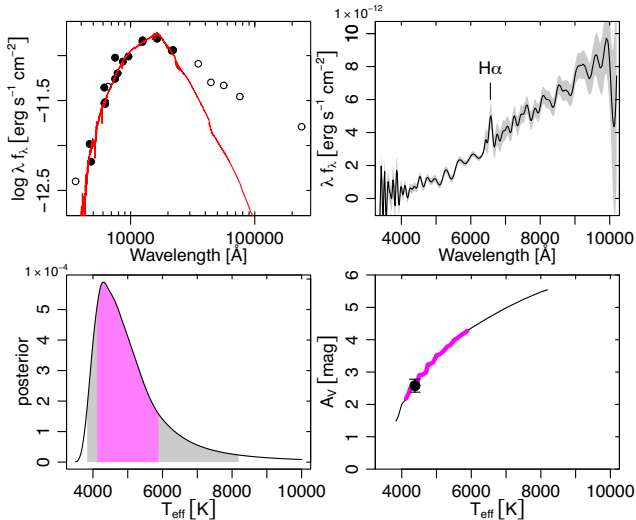


Figure 13. Pre-outburst properties of V1741 Sgr. Top left: The stellar SED. Photometric measurements used in the fit are black points, and those with excess emission are open circles. The maximum-likelihood stellar atmosphere model ($T_{\text{eff}} \sim 4380$ K; $A_V \sim 2.6$ mag) is indicated by the red line. Top right: The Gaia BP/RP spectrum, with the uncertainty envelope in grey. Bottom left: The posterior distribution for T_{eff} . The 68 per cent credible interval is shaded magenta, and the 95 per cent credible interval is shaded grey. Bottom Right: The line illustrates degeneracy between A_V on T_{eff} from SED fitting. The black point indicates the maximum-likelihood parameters, the error bar indicates uncertainty on A_V for a fixed T_{eff} , and the credible intervals are indicated by the magenta (68 per cent) and black (95 per cent) portions of the line.

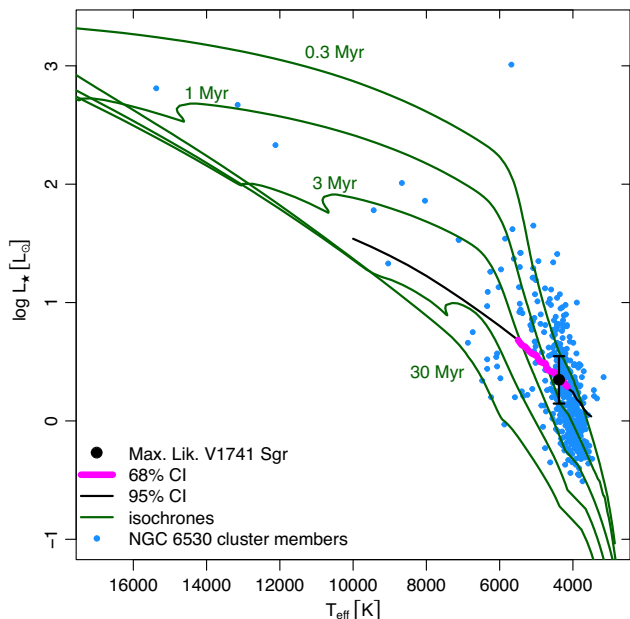


Figure 14. Hertzsprung–Russell diagram for NGC 6530. The plot shows the maximum-likelihood parameters for V1741 Sgr (black point), uncertainty on its L_* for a fixed T_{eff} (error bar), and its 68 per cent (magenta curve) and 95 per cent (black curve) credible intervals given the A_V – T_{eff} degeneracy. Cluster members with Gaia-ESO spectroscopy are indicated by the blue points. Pre-main-sequence isochrones for 0.3–30 Myr (Bressan et al. 2012) are indicated by the green curves.

suggesting that extinction may have decreased during the outburst as has been observed in several other EX Lup-type events (e.g. Lorenzetti et al. 2012). Nevertheless, the broad posterior distributions for A_V mean that this change is not highly statistically significant. For the remainder of the analysis, we will assume our best-estimate A_V values. However, if A_V did not change, the increase in brightness would need to be driven entirely by temperature and surface area increases.

V1741 Sgr lies in the pre-main-sequence region of the Hertzsprung-Russell diagram (Fig. 14), along with other young members of the Lagoon Nebula whose temperatures and luminosities have been obtained from the Gaia-ESO survey (Jackson et al. 2022). Assuming that stars in the Lagoon Nebula have similar ages, the other members can serve as a guide to the most probable (T_{eff} , $\log L$) combination for V1741 Sgr. Our best-fit parameters lie amid the densest group of low-mass Gaia-ESO cluster members, suggesting that they are reasonable estimates. These parameters correspond to a stellar mass of $0.8 M_{\odot}$ and an age of 0.7 Myr in the PARSEC evolutionary models (Bressan et al. 2012). Nevertheless, the uncertainty in T_{eff} and the systematic differences between theoretical evolutionary models (e.g. David et al. 2019; Braun et al. 2021) can cause estimates to vary by a factor of several.

The $H\alpha$ -line flux from the calibrated Gaia BP/RP spectrum is $(2.5 \pm 0.6) \times 10^{-14}$ erg s $^{-1}$ cm $^{-2}$, corresponding to an equivalent width of -52 ± 14 Å. Assuming $A_V = 2.6$ mag, the extinction-corrected line-luminosity would be $(3.4 \pm 0.5) \times 10^{31}$ erg s $^{-1}$. Applying the relation between $H\alpha$ and accretion luminosity from Alcalá et al. (2014) gives

$$\log(L_{\text{acc}}/L_{\odot}) \approx 1.12 \times \log(L_{H\alpha}/L_{\odot}) + 1.5 = -0.9. \quad (2)$$

Then substituting a values of $M_* = 0.8 M_{\odot}$ and $R_* = 2.6 R_{\odot}$ into their equation 1 yields an accretion rate of

$$\dot{M} = \eta \frac{L_{\text{acc}} R_*}{GM_*} = 2 \times 10^{-8} M_{\odot} \text{ yr}^{-1}, \quad (3)$$

where G is the gravitational constant and $\eta = 1.25$ is an approximate correction factor for accreting material falling from a radius of $\sim 5 R_*$ (Alcalá et al. 2014). This \dot{M} is at the high end for quiescent T Tauri stars (Manara et al. 2023).

7 EVOLUTION OF THE SED

7.1 Infrared emission

Infrared photometry can constrain whether brightening is driven by changes in extinction or luminosity (Fig. 15). Lorenzetti et al. (2012) showed that many EX Lup-type outbursts became substantially bluer in both $J - H$ and $H - K$ colours, with colour changes too extreme to be solely temperature effects. Nevertheless, not all EX Lup-type stars in their sample demonstrated this behaviour – notably EX Lup itself became redder in $H - K$ during its 2008 outburst but maintained a nearly constant $J - H$ colour. The NEOWISE light curves for V1741 Sgr showed the source becoming redder during the outburst by $\Delta(W1 - W2) = 0.3 \pm 0.1$ mag (Section 3). This is opposite what would be expected from decreasing extinction, implying that something else is occurring.

V1741 Sgr's mean pre-outburst magnitudes of $J = 13.8$ mag, $H = 12.8$ mag, and $K_s = 12.3$ mag were obtained from VVV. The SED fit in Section 6.2 indicates that the J and H bands are dominated by photospheric emission, whilst the K_s band exhibits some infrared excess. Assuming a pre-outburst extinction of $A_V = 2.6$ mag, the

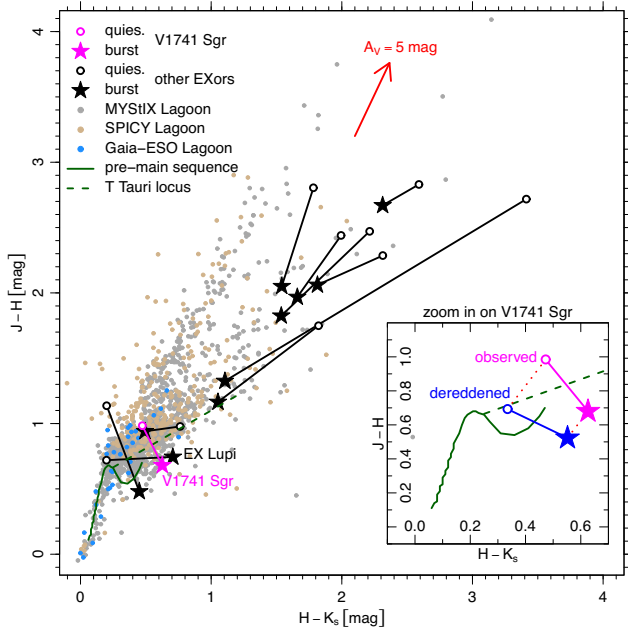


Figure 15. $J - H$ versus $H - K_s$ colours for YSOs, including V1741 Sgr (magenta), other EXOrs (black), and other members of the Lagoon Nebula region (grey: MYStIX; tan: SPICY; light blue: Gaia-ESO). For the outbursters, open circles indicate the quiescent JHK_s colours and star symbols indicate outburst colours. The photometry for the other EXOrs was obtained from Lorenzetti et al. (2012, their table 3). (Note that the sources in their table differ from those in their fig. 1. The JHK_s colours we show are calculated from the flux densities in their table, which we have calibrated to the VVV system.) The plot also indicates intrinsic colours of pre-main-sequence stars (Pecaut & Mamajek 2013), the T Tauri locus (Meyer, Calvet & Hillenbrand 1997), and the reddening vector (Wang & Chen 2019). The inset (bottom right) shows an expanded view of the observed (magenta) and dereddened (blue) colours of V1741 Sgr.

dereddened photometry is $J_{\text{dered}} = 13.2$ mag, $H_{\text{dered}} = 12.5$ mag, and $K_{s, \text{dered}} = 12.1$ mag.

To characterize the near-infrared changes during the outburst, we generated synthetic photometry from the SpeX spectrum, using the VISTA JHK_s filter profiles. This yielded values of $J = 12.0$ mag, $H = 11.3$ mag, and $K_s = 10.7$ mag. Assuming an outburst extinction of $A_V = 1.4$ mag, the dereddened magnitudes are $J_{\text{dered}} = 11.7$ mag, $H_{\text{dered}} = 11.1$ mag, and $K_{s, \text{dered}} = 10.6$ mag. These correspond to a factor of 3.6–4 increase in luminosity in this near-infrared spectral region, meaning that the accretion luminosity dominates over the stellar photospheric emission at all wavelengths observed.

On the $J - H$ versus $H - K_s$ colour–colour diagram (Fig. 15), the outburst shifted the star to the lower right, implying that the transition from becoming bluer during outburst to becoming redder during outburst happened around $\sim 1.6 \mu\text{m}$ (H band). The star started on the T Tauri locus from Meyer, Calvet & Hillenbrand (1997), but this shift brought the star below the line. This behaviour differs from most of the sources examined by Lorenzetti et al. (2012), which tend to get bluer in both colours. However, a few sources from the Lorenzetti et al. (2012) sample with bluer initial colours also defy this trend. A possible explanation is that the bluer sources start less embedded, limiting the impact of changes in extinction.

The dereddened outburst colours of $(J - H)_{\text{dered}} = 0.52$ mag and $(H - K_s)_{\text{dered}} = 0.55$ mag are similar, indicating that the outbursting

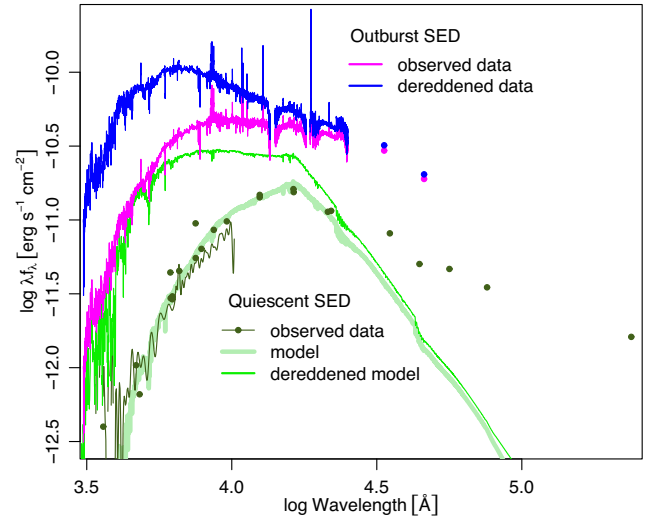


Figure 16. SEDs for V1741 Sgr before and during the outburst, with dereddening corrections applied, assuming $A_V = 2.6$ mag in quiescence and $A_V = 1.4$ mag during the outburst. The pre-outburst SED is constructed from multisurvey photometry and the Gaia BP/RP spectrum, while the outburst SED is constructed from the LRIS + SpeX spectroscopy and NEOWISE.

source’s SED has a nearly constant spectral index of

$$\alpha = \frac{d \log \lambda f_\lambda}{d \log \lambda} \approx 1.7 (J - K_s)_{\text{dered}} - 2.6 = -0.7 \quad (4)$$

in the near-infrared. When comparing to stellar atmosphere models from the PHOENIX library (Husser et al. 2013), the outburst’s intrinsic $J - H$ colour corresponds to $T_{\text{eff}} = 4400$ K for their $\log g = 0$ models, $T_{\text{eff}} = 4600$ K for their $\log g = 1$ models, or $T_{\text{eff}} = 4700$ K for their $\log g = 2$ models. These temperature constraints on the outbursting source are consistent with the temperature ranges estimated from the absorption features detected in the optical and near-infrared.

7.2 Accretion luminosity

Examination of the SEDs of V1741 Sgr revealed that the source brightened over the full wavelength range in both observed and dereddened flux. The smallest increase was around $\sim 1.6 \mu\text{m}$ (H band), where a factor of ~ 3.6 increase in the flux density was observed after applying the dereddening corrections (Fig. 16). Assuming our best-fitting stellar and outburst parameters, a factor of ~ 2 increase in emitting stellar surface area would be needed to explain this H -band brightening. Additionally, a larger surface area during the outburst decline is indicated by TiO absorption features (April 2023), whose depth in flux units is significantly greater than the stellar continuum from the post-outburst (August 2023) spectrum.

The outburst’s total accretion luminosity may be estimated by integrating the dereddened outburst SED and subtracting the stellar luminosity. We integrated this SED (blue curve in Fig. 16) over the observed range, from ~ 3000 to $46\,000 \text{ \AA}$ using linear interpolation where there are gaps in the data. Although these integration limits do not include portions of the ultraviolet and infrared, the intrinsic spectrum is decreasing in both extremes, suggesting that the omitted spectral regions only provide small contributions to the bolometric luminosity. The accretion luminosity calculated in this way is $L_{\text{acc}} = 5 L_\odot$.

Using equation (3) and assuming the stellar parameters from Section 6.2, we calculate a peak outburst accretion rate of $\dot{M} \approx 6 \times 10^{-7} M_{\odot} \text{ year}^{-1}$. If we integrate the accretion over the full duration of the outburst, assuming that the accretion rate is proportional to the r -band flux increase, the total mass accreted is $6 \times 10^{-7} M_{\odot}$, or $0.2 M_{\oplus}$.

The calculations above assumed A_V estimates that indicate a slight decrease during the outburst (Section 6.2). Here, we briefly examine the alternative scenario that A_V did not change, remaining constant at $A_V = 1.4$ mag. This would imply slightly larger changes in both temperature and dereddened H band flux (see Sections 5.2, 6.2, and 7.1). These approximately compensate for each other, so the estimated change in emitting surface area would still be a factor of ~ 2 .

8 DISCUSSION

In broad terms, EX Lup-type outburst spectra resemble scaled-up T Tauri spectra (Fischer et al. 2023). However, the detection of low-gravity absorption lines from Ba II and Sr II (Section 4) may suggest a difference in the structure of V1741 Sgr's emitting regions compared to typical T Tauri stars.

Explaining V1741 Sgr's continuum brightening also requires a change in emission structure during outburst. In the standard T Tauri model, accretion excess (e.g. veiling) comes from hotspots on the stellar surface. However, hotspots are insufficient to explain the brightening of V1741 Sgr, which requires an emitting area ~ 2 times larger than the stellar surface (Section 7.2). The impossibility of achieving the brightening via hotspots is underlined by the change in the outburst spectral type from K to early M during the beginning of the decline. When the early-M-type spectrum was observed, the star was still a factor of several brighter than its quiescent level, meaning that the spectrum was still dominated by the outburst and not the star (Fig. 9). However, the ~ 3600 K implied by the spectrum is much cooler than expected from accretion hotspots. Furthermore, the early-M spectral type is cooler than the final post-outburst stellar spectrum, so, to outshine the star, this gas must have had a larger surface area (Fig. 10). We can also rule out reprocessed emission from the disc or disc wall as the main contributor to the outburst continuum because dust produces a featureless spectrum, not the evolving absorption spectrum witnessed. We propose the alternative that the spectrum is dominated by circumstellar gas, which also explains the low-gravity features.

The puzzling appearance then disappearance of the TiO bands during the transition of the star from outburst to quiescence (Figs 9 and 10) can be explained by the above scenario. At the outburst peak, the circumstellar gas would have a photospheric temperature of ~ 4750 K. This gas would start to cool during the outburst decay, leading to the cooler spectrum. Eventually, the circumstellar gas would fade sufficiently for the stellar spectrum, with a higher temperature, to reemerge.

In FU Ori outbursts, the luminosity is expected to originate from viscously heated discs. However, models based on a disc with a Kenyon, Hartmann & Hewett (1988) temperature profile cannot reproduce V1741 Sgr's SED. Using an implementation of this model by Rodriguez & Hillenbrand (2022), it is impossible to simultaneously fit the blue and near-infrared portions of the source owing to the model's overestimation of the near-infrared emission. This is not surprising, given that the EX Lup phenomenon is generally attributed to changes near the star's magnetosphere rather than an increase in mass accretion through the whole disc (Sicilia-Aguilar et al. 2012). Given that the gas contributing to the increased

continuum emission has a surface area a factor of several times the star's surface area, this gas could be distributed within either the stellar magnetosphere or in a small portion of the innermost disc.

To investigate whether it is plausible that the increased continuum emission resulted from optically thick infalling gas in the magnetosphere, we performed a rough optical depth calculation. In our toy model, gas falls onto the star with an accretion rate $\dot{M} = 6 \times 10^{-7} M_{\odot} \text{ yr}^{-1}$, from a radius $r = 5R_*$, with a free-fall time of $t \approx (\pi^2 r^3 / 8GM_*)^{1/2} \approx 1$ d. We further assume that this gas has a surface area (in projection) twice that of the star ($A \approx 2\pi R_*^2$). The mean surface density of this material will be $\Sigma \approx \dot{M} t A^{-1} \sim 16 \text{ g cm}^{-2}$. The opacity of 4750 K gas is $\kappa \approx 0.001\text{--}0.01 \text{ cm}^2 \text{ g}^{-1}$ depending on volume density (ÆSOPUS⁸ 2.0; Marigo & Aringer 2009; Marigo et al. 2022). This suggests that, if the infalling gas were distributed over the required surface area, it would be moderately optically thin and incapable of producing the increased continuum emission. Furthermore, the gas would need a temperature structure that generates the observed absorption spectrum. Nevertheless, the significant uncertainties in the toy model mean that such a scenario cannot be definitively ruled out. However, emission from the innermost portion of the gas disc seems a more likely explanation for the increased optical/near-infrared continuum.

To explain the changing mid-infrared spectral index, it may be possible to invoke reprocessed emission alone. In the pre-outburst SED (Section 6.2), the mid-infrared is dominated by reprocessed emission, whilst the near-infrared is dominated by stellar emission. The total reprocessed luminosity of a dust disc will scale proportionally to the total luminosity of the central illuminating source. As V1741 Sgr brightened, the emission of the central source shifted to be dominated by the blue part of the spectrum. If the mid-infrared reprocessed emission increases proportionally to the luminosity of the central source, it would increase faster than the near-infrared, which now contributes a smaller fraction to the total source luminosity. This effect could explain why V1741 Sgr became redder beyond $1.6 \mu\text{m}$. The H^- continuum opacity minimum around $1.6 \mu\text{m}$ (Gray 2005) also affects the relative temperature sensitivity of H -band flux, but this is likely to have been a minor effect owing to the coincidental similarity of the pre- and peak-outburst temperature estimates. Detailed modelling (beyond the scope of this paper) would be necessary to determine if a configuration of circumstellar material can reproduce the specific mid-infrared SED changes undergone by V1741 Sgr during this event.

V1741 Sgr's relatively simple light curve, with onset, plateau, and decay phases lasting several months each, can be explained by the accretion scenario for EX Lup developed by Sicilia-Aguilar et al. (2012). In this scenario, accretion through stable channels in the magnetosphere would yield the rapid onset and recovery of the system and the relatively constant brightness during the high state. V1741 Sgr's light curve is simpler than most other objects in its class, many of which have repeated bursts and outbursts of varying amplitudes or exhibit significant substructure in their outburst light curves (e.g. Aspin et al. 2010; Ninan et al. 2015; Park et al. 2022). However, the small burst seen by PGIR in the month before the main outburst suggests that the outburst began in a gradual and choppy way. This would be consistent with mass release due to accretion instability (D'Angelo & Spruit 2010, 2012; Armitage 2015) but argues against triggering by a sudden event (e.g. a stellar flyby).

Comparison of V1741 Sgr to LkH α 225 S and Gaia 19ajj highlights the diversity of spectra of outbursting YSOs. Differences include

⁸<http://stev.oapd.inaf.it/cgi-bin/aesopus>

V1741 Sgr’s stronger H I and He I lines, stronger O I, and its weakness or lack of many of the emission lines species like Fe I, Mg I, Ti I, or K I. Although CO emission is a defining feature of EX Lup-type outbursts, there can be significant differences between how the bandheads appear, with V1741 Sgr having relatively strong emission. Absorption lines with higher excitation potentials (C I, S I, and P I) are seen in the spectrum of V1741 Sgr, but not LkH α 225 S and Gaia 19ajj. Finally, LkH α 225 S shows some wavelength-temperature dependence but V1741 Sgr does not.

9 CONCLUSION

Our analysis identifies this year-long outburst from V1741 Sgr as an EX Lup-type event of moderate amplitude (~ 3 mag in the optical and 1–2 mag in the infrared). The star is a classical T Tauri star (Section 6.2) on the outskirts of the Lagoon Nebula (Section 6.1), and the outbursting spectrum is characterized by strong atomic (H I, He I, Ca II, and O I) and molecular (CO) emission (Section 4). The spectrum reveals brightening across the entire observed range, from the near-ultraviolet to the mid-infrared, causing a partial flattening of the SED (Section 7.2). Other features common in EX Lup-type objects, such as deeper absorption from wind-sensitive lines and low-gravity absorption features, are also present in this source (Sections 4.1 and 4.2).

The spectral evolution of the outburst from its peak to its decline and, finally, its post-outburst state provides clues about the origin of emission from EX Lup-type sources. The most notable change in V1741 Sgr’s spectrum was the appearance and subsequent disappearance of TiO absorption while it continued to fade (Section 5). The timing of the appearance of the TiO absorption implies that this feature is connected to the outburst rather than the stellar photosphere, supporting our conclusion that circumstellar emission dominates the outburst continuum spectrum (Section 8).

Our observations help build the sample of spectroscopically characterized EX Lup-type events. However, a detailed comparison of spectroscopic features reveals numerous differences between objects (Section 4), suggesting that accretion discs and stellar magnetospheres have a variety of ways to interact. Although outbursts are most common from embedded protostars (Lorenzetti et al. 2012; Audard et al. 2014; Contreras Peña et al. 2017a, b), those from more evolved YSOs, including V1741 Sgr and the prototypical EX Lup, help us understand the later stages of disc evolution, especially during phases when outbursts may affect forming planets.

The basic properties of the star and the outburst are summarized below:

(i) V1741 Sgr was formed on the outskirts of the Lagoon Nebula, near a subcluster designated G5.9-0.9 (Kuhn et al. 2021b), rather than the main NGC 6530 cluster. The star’s Gaia parallax indicates a distance of ~ 1260 pc. Environmental extinction includes $A_V = 0.6$ mag from the foreground and $\Delta A_V = 0.6$ mag from a cloud at the star’s distance (Sections 4.3 and 6.1).

(ii) The pre-outburst SED suggests that the star has an early-to-mid K spectral type and $A_V \sim 2.6$ mag of extinction. This extinction is higher than that of the cloud, indicating a significant intrinsic component. Both near-ultraviolet and mid-infrared excesses are detected. We derive an age $\lesssim 3$ Myr and a quiescent accretion rate of $\sim 2 \times 10^{-8} M_{\odot} \text{ yr}^{-1}$ (Section 6.2).

(iii) The outburst light curve consists of a ~ 60 d rise, a ~ 280 d plateau, then a ~ 110 d decay. The rise followed a sigmoid-like function, with slight lags in the rises at longer wavelengths. The decay was more choppy, with multiple temporary dips (Section 3).

(iv) In the final photometric epochs, after the end of the outburst, the source dimmed to a fainter state than its pre-outburst level.

(v) The outburst caused the SED to become bluer at wavelengths $< 1.6 \mu\text{m}$ and redder at wavelengths $> 1.6 \mu\text{m}$ (Section 7.1). The increased blueness is likely a combination of increased temperature and decreased extinction, whilst the increased redness is likely an increase in reprocessed emission.

(vi) There may have been a moderate decrease in extinction during the outburst ($\Delta A_V \sim -1.2$ mag). Nevertheless, this decrease is insufficient to explain the outburst’s colour or brightness in either the optical (Section 3.3) or infrared (Section 7.1). Stochastic variability before the outburst and during the plateau is consistent with variable extinction.

(vii) In the LRIS spectrum (Oct 2022), absorption features indicate a $\sim K2$ spectral type (~ 4750 K), with no evidence for a wavelength-temperature dependence (Sections 4.1 and 4.2). The strengths of low-gravity absorption features (Ba II and Sr II) suggest that these lines were not formed on the stellar surface.

(viii) Sequential spectroscopic observations revealed an evolving spectral type (Section 5). In the first Kast spectra (April 2023), absorption features, especially TiO, indicated an M1–M2 spectral type (~ 3600 K). In the final Kast spectrum (August 2023), the disappearance of TiO absorption and the absence of MgH implied a spectral type of K5 or earlier ($T \gtrsim 4140$ K).

(ix) Analysis of the H emission lines with the Kwan & Fischer (2011) model indicates the additional presence of optically thin ~ 5000 K gas (Section 4.4).

(x) The relative strengths of H I, He I, Ca II, O I, Fe I, Mg I, Ti I, Na I, K I, and CO features differ notably between several compared EX Lup-like outbursts. Strong Fe emission, which is often seen from accreting T Tauri stars, only emerged once the outburst faded.

(xi) The accretion luminosity in the source’s high state is $\sim 5 L_{\odot}$, corresponding to an outburst accretion rate of $\sim 6 \times 10^{-7} M_{\odot} \text{ yr}^{-1}$. At this rate, the event would have deposited $0.2 M_{\oplus}$ onto the star (Section 7.2).

Combining large YSO catalogues with sky-monitoring surveys will likely improve the count statistics of these events. For example, as of December 2023, there have been > 300 Gaia alerts for sources in the SPICY catalogue, including other possible EX Lup-like events (e.g. Kuhn et al. 2023a). The growing lists of YSO outbursts will likely fill in the spectroscopic parameter space and improve our understanding of typical properties and how these events vary.

ACKNOWLEDGEMENTS

We thank Calum Morris and Zhen Guo for valuable comments, Leigh Smith for access to proprietary VVV data products, and Facundo Pérez Paolino for participation in the Palomar observation. We also thank the referee for thorough and helpful reviews of this paper. We acknowledge the significant cultural role and reverence that the summit of Maunakea has within the indigenous Hawaiian community and that we are most fortunate to have the opportunity to conduct observations from this mountain. IRTF is operated by the University of Hawaii under contract 80HQTR19D0030 with NASA. The W. M. Keck Observatory is operated as a scientific partnership among the California Institute of Technology, the University of California, and NASA. The Observatory was made possible by the generous financial support of the W. M. Keck Foundation. The Kast Double Spectrograph was made possible by a generous gift from William and Marina Kast. We acknowledge ESA Gaia, the Data Processing and Analysis Consortium, and the Photometric Science

Alerts Team. ZTF is led by the California Institute of Technology, USA, supported by the National Science Foundation under Grant No. AST-2034437, and includes IPAC, USA; Los Alamos National Laboratory, USA; University of Maryland, USA; the University of Wisconsin at Milwaukee, USA; University of Washington, USA; Oskar-Klein Center of the University of Stockholm, Sweden; DESY and Humboldt University of Berlin, Germany; Weizmann Institute of Science, Israel; and the University System of Taiwan, Taiwan.

DATA AVAILABILITY

The spectra from Table 1 and the TAGRA and PGIR light curves are provided online as supplementary material. Other data sets are publicly available from the sources in Section 2.

REFERENCES

- Alam S. et al., 2015, *ApJS*, 219, 12
- Alcalá J. M. et al., 2014, *A&A*, 561, A2
- Armitage P. J., 2015, preprint (arXiv:1509.06382)
- Aspin C., Reipurth B., Herczeg G. J., Capak P., 2010, *ApJ*, 719, L50
- Audard M. et al., 2014, in Beuther H., Klessen R. S., Dullemond C. P., Henning T., eds, *Protostars and Planets VI*. Univ. Arizona Press, Tucson, AZ, p. 387
- Azevedo R., Calvet N., Hartmann L., Folha D. F. M., Gameiro F., Muzerolle J., 2006, *A&A*, 456, 225
- Bellm E. C. et al., 2019, *PASP*, 131, 018002
- Benjamin R. A. et al., 2003, *PASP*, 115, 953
- Bohlin R. C., Mészáros S., Fleming S. W., Gordon K. D., Koekemoer A. M., Kovács J., 2017, *AJ*, 153, 234
- Borchers H. W., 2022, *pracma: Practical Numerical Math Functions*. Available at: <https://CRAN.R-project.org/package=pracma>
- Bouvier J. et al., 2003, *A&A*, 409, 169
- Bowen I. S., 1947, *PASP*, 59, 196
- Braun T. A. M., Yen H.-W., Koch P. M., Manara C. F., Miotello A., Testi L., 2021, *ApJ*, 908, 46
- Bressan A., Marigo P., Girardi L., Salasnich B., Dal Cero C., Rubele S., Nanni A., 2012, *MNRAS*, 427, 127
- Broyden C. G., 1970, *IMA J. Appl. Math.*, 6, 76
- Cardelli J. A., Clayton G. C., Mathis J. S., 1989, *ApJ*, 345, 245
- Carey S. J. et al., 2009, *PASP*, 121, 76
- Carvalho A. S., Hillenbrand L. A., 2022, *ApJ*, 940, 156
- Chambers K. C. et al., 2016, preprint (arXiv:1612.05560)
- Churchwell E. et al., 2009, *PASP*, 121, 213
- Connelley M. S., Reipurth B., 2018, *ApJ*, 861, 145
- Contreras Peña C. et al., 2017a, *MNRAS*, 465, 3011
- Contreras Peña C. et al., 2017b, *MNRAS*, 465, 3039
- Contreras Peña C. et al., 2023a, *J. Korean Astron. Soc.*, 56, 253
- Contreras Peña C. et al., 2023b, *MNRAS*, 521, 5669
- Covey K. R. et al., 2011, *AJ*, 141, 40
- Cruz-Sáenz de Miera F. et al., 2022, *ApJ*, 927, 125
- Cushing M. C., Vacca W. D., Rayner J. T., 2004, *PASP*, 116, 362
- D'Angelo C. R., Spruit H. C., 2010, *MNRAS*, 406, 1208
- D'Angelo C. R., Spruit H. C., 2012, *MNRAS*, 420, 416
- David T. J., Hillenbrand L. A., Gillen E., Cody A. M., Howell S. B., Isaacson H. T., Livingston J. H., 2019, *ApJ*, 872, 161
- De Angeli F. et al., 2023, *A&A*, 674, A2
- De K. et al., 2020, *PASP*, 132, 025001
- Drew J. E. et al., 2014, *MNRAS*, 440, 2036
- Fang M., Hillenbrand L. A., Kim J. S., Findeisen K., Herczeg G. J., Carpenter J. M., Rebull L. M., Wang H., 2020, *ApJ*, 904, 146
- Fazio G. G. et al., 2004, *ApJS*, 154, 10
- Fischer W. J., Hillenbrand L. A., Herczeg G. J., Johnstone D., Kospal A., Dunham M. M., 2023, in Inutsuka S., Aikawa Y., Muto T., Tomida K., Tamura M., eds, *ASP Conf. Ser. Vol. 534, Protostars and Planets VII*. Astron. Soc. Pac., San Francisco, p. 355
- Fletcher R., 1970, *Comput. J.*, 13, 317
- Flewelling H. A. et al., 2020, *ApJS*, 251, 7
- Fouqué P. et al., 2000, *A&AS*, 141, 313
- Fraley C., Raftery A. E., 2002, *J. Am. Stat. Assoc.*, 97, 611
- Gaia Collaboration, 2016, *A&A*, 595, A1
- Gaia Collaboration, 2021, *A&A*, 649, A1
- Giannini T. et al., 2022, *ApJ*, 929, 129
- Goldfarb D., 1970, *Math. Comput.*, 24, 23
- Golub G. H., Van Loan C. F., 1980, *SIAM J. Numerical Anal.*, 17, 883
- Graham M. J. et al., 2019, *PASP*, 131, 078001
- Gray D. F., 2005, *The Observation and Analysis of Stellar Photospheres*. Cambridge Univ. Press, Cambridge, <http://www.cambridge.org/9780521858162>
- Gray R. O., Corbally C. J., 2009, *Stellar Spectral Classification*. Princeton Univ. Press, Princeton, NJ
- Green G. M., Schlafly E., Zucker C., Speagle J. S., Finkbeiner D., 2019, *ApJ*, 887, 93
- Guo Z. et al., 2020, *MNRAS*, 492, 294
- Gutermuth R. A., Heyer M., 2015, *AJ*, 149, 64
- Hamann F., Persson S. E., 1992, *ApJS*, 82, 247
- Hartmann L., Kenyon S. J., 1996, *ARA&A*, 34, 207
- Hartmann L., Herczeg G., Calvet N., 2016, *ARA&A*, 54, 135
- Herczeg G. J., Hillenbrand L. A., 2014, *ApJ*, 786, 97
- Herter T. L., Henderson C. P., Wilson J. C. et al., 2008, in *Proc. SPIE*, 7014, 70140X
- Hillenbrand L. A., Rodriguez A. C., 2022, *Res. Notes Am. Astron. Soc.*, 6, 6
- Hillenbrand L. A. et al., 2018, *ApJ*, 869, 146
- Hillenbrand L. A., Reipurth B., Connelley M., Cutri R. M., Isaacson H., 2019a, *AJ*, 158, 240
- Hillenbrand L. A. et al., 2019b, *ApJ*, 874, 82
- Hillenbrand L. A. et al., 2021, *AJ*, 161, 220
- Hillenbrand L. A., Isaacson H., Rodriguez A. C., Connelley M., Reipurth B., Kuhn M. A., Beck T., Perez D. R., 2022a, *AJ*, 163, 115
- Hillenbrand L. A., Kiker T. J., Gee M., Lester O., Braunfeld N. L., Rebull L. M., Kuhn M. A., 2022b, *AJ*, 163, 263
- Hodapp K. W. et al., 2019, *AJ*, 158, 241
- Hodgkin S. T. et al., 2021, *A&A*, 652, A76
- Hodgkin S. T. et al., 2022, *Transient Name Server Discovery Report*, 2022-2604, 1
- Husser T. O., Wende-von Berg S., Dreizler S., Homeier D., Reiners A., Barman T., Hauschildt P. H., 2013, *A&A*, 553, A6
- Jackson R. J. et al., 2022, *MNRAS*, 509, 1664
- Jeffries R. D. et al., 2023, *MNRAS*
- Kastner S. O., Bhatia A. K., 1995, *ApJ*, 439, 346
- Kenyon S. J., Hartmann L., Hewett R., 1988, *ApJ*, 325, 231
- Kirkpatrick J. D., Henry T. J., McCarthy Donald W. J., 1991, *ApJS*, 77, 417
- Kóspál Á. et al., 2011, *ApJ*, 736, 72
- Kóspál Á. et al., 2023, *ApJ*, 945, L7
- Kuhn M. A., Hillenbrand L. A., Sills A., Feigelson E. D., Getman K. V., 2019, *ApJ*, 870, 32
- Kuhn M. A., de Souza R. S., Krone-Martins A., Castro-Ginard A., Ishida E. O., Povich M. S., Hillenbrand L. A., 2021a, *ApJS*, 254, 33
- Kuhn M. A. et al., 2021b, *A&A*, 651, L10
- Kuhn M. A., Hillenbrand L. A., Feigelson E. D., Fowler I., Getman K. V., Broos P. S., Povich M. S., Gromadzki M., 2022a, *ApJ*, 937, 46
- Kuhn M. A. et al., 2022b, *Astron. Telegram*, 15721, 1
- Kuhn M. A., Benjamin R. A., Ishida E. E. O., de Souza R. S., Peloton J., Veneri M. D., 2023a, *Res. Notes Am. Astron. Soc.*, 7, 57
- Kuhn M. A. et al., 2023b, *AJ*, 165, 3
- Kwan J., Fischer W., 2011, *MNRAS*, 411, 2383
- Lasker B. M., Sturch C. R., McLean B. J., Russell J. L., Jenkner H., Shara M. M., 1990, *AJ*, 99, 2019
- Lawrence A. et al., 2007, *MNRAS*, 379, 1599
- Lindgren L. et al., 2021a, *A&A*, 649, A2
- Lindgren L. et al., 2021b, *A&A*, 649, A4
- Lorenzetti D. et al., 2012, *ApJ*, 749, 188

- Lucas P. W. et al., 2008, *MNRAS*, 391, 136
- Lucas P. W. et al., 2020, *MNRAS*, 499, 1805
- Magakian T. Y., Movsessian T. A., Andreasyan H. R., Gevorgyan M. H., 2019, *A&A*, 625, A13
- Mainzer A. et al., 2011, *ApJ*, 731, 53
- Manara C. F., Ansdell M., Rosotti G. P., Hughes A. M., Armitage P. J., Lodato G., Williams J. P., 2023, in Inutsuka S., Aikawa Y., Muto T., Tomida K., Tamura M., eds, ASP Conf. Ser. Vol. 534, Protostars and Planets VII. Astron. Soc. Pac., San Francisco, p. 539
- Marigo P., Aringer B., 2009, *A&A*, 508, 1539
- Marigo P., Aringer B., Girardi L., Bressan A., 2022, *ApJ*, 940, 129
- Merrill P. W., 1943, *PASP*, 55, 242
- Meyer M. R., Calvet N., Hillenbrand L. A., 1997, *AJ*, 114, 288
- Miller J. S., Stone R. P. S., 1993, Technical Report, Lick Obs. Tech. Rep. 66. Lick Observatory, Santa Cruz, CA
- Minniti D. et al., 2010, *New Astron.*, 15, 433
- Montegriffo P. et al., 2023, *A&A*, 674, A3
- Ninan J. P. et al., 2015, *ApJ*, 815, 4
- Oke J. B. et al., 1995, *PASP*, 107, 375
- Park S. et al., 2022, *ApJ*, 941, 165
- Pecaut M. J., Mamajek E. E., 2013, *ApJS*, 208, 9
- Poppenhaeger K. et al., 2015, *AJ*, 150, 118
- Prochaska J. et al., 2020, *J. Open Source Softw.*, 5, 2308
- Prochaska J. X. et al., 2023, pypeit/PypeIt: Version 1.13.0, Zenodo, available at: <https://doi.org/10.5281/zenodo.8006579>
- R Core Team, 2022, R: A Language and Environment for Statistical Computing. R Foundation for Statistical Computing, Vienna, Austria, available at: <https://www.R-project.org/>
- Rayner J. T., Toomey D. W., Onaka P. M., Denault A. J., Stahlberger W. E., Vacca W. D., Cushing M. C., Wang S., 2003, *PASP*, 115, 362
- Reipurth B., 1990, in Mirzozian L. V., Pettersen B. R., Tsvetkov M. K., eds, Vol. 137, Flare Stars in Star Clusters, Associations and the Solar Vicinity. Kluwer, Dordrecht, p. 229
- Rodrigo C., Solano E., 2020, in XIV.0 Scientific Meeting (virtual) of the Spanish Astronomical Society. p. 182
- Rodrigo C., Solano E., Bayo A., 2012, SVO Filter Profile Service Version 1.0, IVOA Working Draft
- Rodríguez A. C., Hillenbrand L. A., 2022, *ApJ*, 927, 144
- Sale S. E. et al., 2009, *MNRAS*, 392, 497
- Scrucca L., Fop M., Murphy T. B., Raftery A. E., 2016, *R J.*, 8, 205
- Semkov E., 2023, *Bulgarian Astronomical Journal*, DSc dissertation, Institute of Astronomy and NAO of the Bulgarian Academy of Sciences, 39, 94
- Shanno D. F., 1970, *Math. Comput.*, 24, 647
- Sharon C., Hillenbrand L., Fischer W., Edwards S., 2010, *AJ*, 139, 646
- Sicilia-Aguilar A. et al., 2012, *A&A*, 544, A93
- Skrutskie M. F. et al., 2006, *AJ*, 131, 1163
- Teodorani M., Errico L., Vittone A. A., Giovannelli F., Rossi C., 1997, *A&AS*, 126, 91
- Walker M. F., 1957, *ApJ*, 125, 636
- Wang S., Chen X., 2019, *ApJ*, 877, 116
- Wang S., Li A., Jiang B. W., 2015, *ApJ*, 811, 38
- Wang T., Li J., Mace G. M., Ji T., Jiang N., Zhu Q., Fang M., 2023, *ApJ*, 957, 8
- Werner M. W. et al., 2004, *ApJS*, 154, 1
- Wolk S. J. et al., 2018, *AJ*, 155, 99
- Wright N. J. et al., 2019, *MNRAS*, 486, 2477

SUPPORTING INFORMATION

Supplementary data are available at *MNRAS* online.

SupplementaryMaterial.zip

Please note: Oxford University Press is not responsible for the content or functionality of any supporting materials supplied by the authors. Any queries (other than missing material) should be directed to the corresponding author for the article.

This paper has been typeset from a $\text{\TeX}/\text{\LaTeX}$ file prepared by the author.